International Journal of Heat and Mass Transfer 235 (2024) 126189

Contents lists available at ScienceDirect

International Journal of Heat and Mass Transfer

journal homepage: www.elsevier.com/locate/ijhmt

Flow boiling in a rectangular micro/mini channel with self-rewetting and non-rewetting fluids

Mandi Venter [a], Arif Widyatama [b,c], Jaco Dirker [a,*], Khellil Sefiane [b]

[a] Department of Mechanical and Aeronautical Engineering, Faculty of Engineering, Clean Energy Research Group, University of Pretoria, Lynnwood Road, Hatfield, 0028, Pretoria, South Africa
[b] School of Engineering, University of Edinburgh, King's Buildings, Mayfield Road, Edinburgh EH9 3JL, Scotland, United Kingdom
[c] Department of Mechanical & Industrial Engineering, Faculty of Engineering, Gadjah Mada University, Jalan Grafika No.2, Yogyakarta, 55281, Indonesia

ARTICLE INFO

Keywords:
Flow-boiling
Micro/mini channel
Heat transfer coefficient
Flow visualisation
Self-rewetting
Binary mixture
Marangoni effect
Surface tension

ABSTRACT

In this experimental investigation the influence of self-rewetting during flow boiling was studied in a horizontal microchannel during one-sided uniform heating. The channel had a width and height of 6 mm and 0.3 mm respectively. Local wall temperature and direct in-time flow visualisation was performed. The working fluids under consideration included water as base reference, pure 1-butanol, pure ethanol, dilute butanol-water self-rewetting mixtures, and a dilute ethanol-water binary mixture. Tests were conducted at mass fluxes of 10, 15 and 25 kg/m^{2}s, over a range of heat fluxes to produce both single phase and two-phase quasi steady state flow data. Within the wall temperature ranges of interest, the butanol-water mixtures (5 % and 7 % by volume butanol) had surface tension characteristics that would draw liquid toward local wall hotspots. Local and average wall temperatures and heat transfer coefficients were obtained and considered against the governing flow pattern visualisations. In contrast to the other fluids, the self-rewetting butanol-water mixtures exhibited significantly more stable flow and more predictable saturation flow boiling heat transfer coefficient trends across all heat fluxes under consideration. At the lowest mass flux, it was found that an increase in the heat flux resulted in an improvement in the self-rewetting fluids heat transfer performance, while at higher mass fluxes this dependence was diminished. Across all mass fluxes and heat fluxes the 5 % butanol-water outperformed its 7 % butanol-water counterpart. The tendency of self-rewetting to reduce local dry-out, even at low mass fluxes are demonstrated.

1. Introduction

Flow boiling is an advanced heat transfer mechanism, occurring within a flow passage, where a fluid undergoes phase change whilst experiencing bulk fluid motion. It is an important heat transfer method used in thermal management applications in several industries including but not limited to, computer cooling, refrigeration applications, power plants and concentrated thermal solar systems [1-3].

Extensive research has been conducted on flow boiling behaviour and heat transfer in large-diameter flow passages as it is commonly used in power cycles and other mainstream industrial processes. However, because of bubble confinement, the heat transfer mechanism and flow boiling behaviour in small-scale passages differ from those realised at larger scales. Depending on the channel dimensions and working fluid properties, hydraulic diameters and dimensionless numbers are often used to classify channels as either macro-, mini- or microchannels [4,5]. However, due to inconsistencies in the literature, it is often considered reasonable to assume that a channel with a hydraulic diameter of <1 mm may be classified as a microchannel [6].

The respective channel classifications exhibit different dominating flow effects that govern the heat transfer mechanism. Macro-channels are predominantly affected by gravity, whilst surface tension effects become more significant in microchannels and mini-channels. The relative importance of buoyancy and shear forces is, however, influenced by the operating mass flux as well as the two-phase flow regime. At low mass fluxes (with lower fluid velocities), buoyancy-driven flow and gravitational effects can become dominant.

Due to the rapid advancement and more stringent performance requirements associated with the miniaturization of electronic devices, enhanced cooling techniques that adhere to small sizing constraints become imperative. Microchannel flow boiling is considered one of the most promising cooling methods for high heat flux devices due to their ability to sustain high heat transfer rates with only small variations in

* Corresponding author at: Department of Mechanical and Aeronautical Engineering, University of Pretoria, South Africa.
E-mail address: jaco.dirker@up.ac.za (J. Dirker).

https://doi.org/10.1016/j.ijheatmasstransfer.2024.126189
Received 8 February 2024; Received in revised form 10 August 2024; Accepted 8 September 2024
Available online 24 September 2024

Nomenclature

A_h	Heated surface area, m^2
C_p	Specific heat capacity, J/kgK
f	Heat loss characteristic function, W
g	Acceleration of gravity, m/s^2
G	Mass flux, kg/m^2s
h	Specific enthalpy, J/kg
h_{fg}	Specific latent heat of vaporisation, J/kg
H	Microchannel inner height, m
I	Electric Current, A
k_w	Wall thermal conductivity, W/mK
L	Length, m
L_h	Microchannel heated length, m
$\dot{m}$	Mass flow rate, kg/s
n	Control volume index number
P	Pressure, Pa
$\dot{q}$	Effective heat flux, W/m^2
$\dot{Q}$	Effective heat transfer rate, W
$\dot{Q}_{input}$	Heat input rate, W
$\dot{Q}_{loss}$	Heat loss rate, W
R_{wire}	Wire electrical resistance, Ω
t	Time, s
T	Temperature, °C
$\overline{T}$	Spatial average temperature, °C
T_0	Environmental temperature, °C
T_s	Surface temperature, °C
T_{sat}	Saturation temperature, °C
t_w	Microchannel wall thickness, m
U	Voltage input, V
$\dot{V}$	Volumetric flow rate, m^3/s
W	Microchannel inner width, m
z	Axial position, m

Greek letters

α	Heat transfer coefficient, W/m^2K
Δz	Control volume axial length, m
γ	Fluid property placeholder
η	Moles
ρ	Density, kg/m^3
σ	Surface tension, N/m
χ	Thermodynamic vapour quality

Subscripts

0	Environmental condition, or to the outside
ave	Average property
f	Fluid property
i	Property of the major component in a solution (solute)
ii	Property of the minor component in a solution (solvent)
in	Inlet property
l	Liquid property
mix	Mixture property
out	Outlet property

surface temperature. In comparison, better axial temperature uniformity is obtained than found with single-phase flow cooling schemes [1].

For rectangular channels, the increased heat transfer rates are not only attributable to the phase change mechanism, but also to the very high surface area to volume ratio [7]. Accordingly, microchannel flow boiling is useful for process intensification, recovery of low-grade waste energy and improving overall system performance [7]. However, due to its complexity and dependence on multiple parameters, microchannel flow boiling is not yet understood fully, leading to delays in implementation.

Dominant parameters influencing flow boiling dynamics and the heat transfer mechanism include the size and geometry of the internal flow passage, the working fluid properties, the fluid mass flux [8], saturation pressure [9], applied heat flux [10,11] and the configuration of the channel. The channel geometry is closely related to the cross-sectional profile, which usually ranges from circular to approximately rectangular. Rectangular channels occur over a wide range of aspect ratios (width-to-height) of between 0.33 and 20. The operating conditions also play a key role in the flow boiling development and behaviour. The working fluid inlet temperature may range from subcooled to saturated conditions, whilst the combination of the mass and heat flux causes different flow boiling regimes and vapour qualities. The mass flux also influences the significance of surface tension and gravity effects.

Generally, the fluid itself is selected according to the specific requirements of an applications based on its thermodynamic and fluid properties. Some common fluids that have been considered in literature include pure water [12], alcohols [13], refrigerants [14], hydrocarbons [15,16] and multicomponent mixtures [17]. Dilute aqueous solutions of alcohols, especially those with molecular structures consisting of four or more carbon atoms have recently received attention [18-21]. Compared to most other fluids whose surface tension degrades linearly with increased temperatures [19], such mixtures have a nonlinear surface tension profile, leading to increased surface tension at elevated temperatures. As an example, the surface tension profiles for two dilute butanol-water mixtures are shown in Fig. 1 (obtained from three sources [18,22,23] and verified against compiled data sets from various previous studies found on Springer Materials [24]). At temperature above 60 °C, localised surface tension can surpass that of neighbouring cooler regions, causing liquid to be drawn inward toward hot surface regions [19,25]. By correctly harnessing such surface tension characteristics, the resulting self-rewetting action can improve two-phase heat transfer performance [19,20] by reducing dry-out.

Due to the applicability of microchannel flow boiling as a thermal management solution, the investigation and development of a fundamental understanding of the heat transfer mechanisms and operational limits are considered imperative [1]. As a result, several research studies have been conducted on single microchannels as well as on heat sinks with multiple channels. These studies considered different variables, including various working fluids, channel wall materials, cross-sectional profiles, hydraulic diameters, hydrodynamic confinement effects, channel orientations and mass and heat flux combinations [26,27].

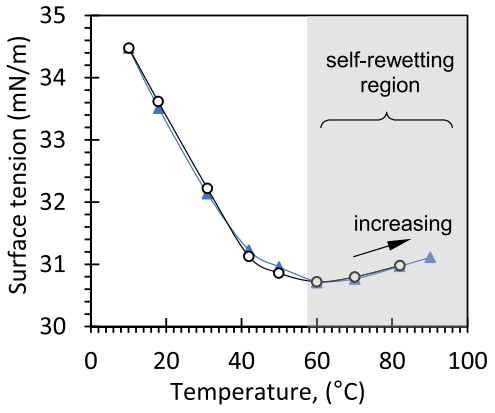

Fig. 1. Surface tension profiles for dilute butanol-water mixtures at 5 % and 7 % volume to volume concentrations.

Although some headway has been made to describe the flow boiling phenomenon, several fundamental issues require even deeper understanding of local bubble behaviours. Little agreement between researchers exists on how the operational conditions, channel geometrical parameters and working fluid properties influence the heat transfer rates and bubble dynamics. Furthermore, the contributions of nucleate and convective boiling related to the different flow regimes remain unresolved. Due to flow boiling inherently being chaotic and susceptible to flow instability, investigations are further complicated by flow instability intensity, which in itself, is also dependent on various parameters. In order to achieve increased heat transfer performance, further experimental investigations are needed.

Although pure water, pure ethanol and ethanol-water binary mixtures have been considered by several researchers [7,19,21,28-33], only a limited number of research studies have been performed with 1-butanol and aqueous 1-butanol self-rewetting fluids [18-22,31]. Table 1 provides a summary of some of the previous research studies conducted with different fluids, specifically focussing on aqueous-alcohol solutions.

Of the studies included in Table 1 that considered butanol-water and ethanol-water mixtures, some considered circular tubes only ([18,19,30,31]), or did not study actual flow boiling ([21]), or did not include binary mixtures such as ethanol-water ([20,22]). Based on the relatively few studies on high aspect-ratio micro/mini channels, and the lack of clarity on how surface tension affects the flow boiling heat transfer performance at low mass flux conditions, additional experimental exploration is needed.

High aspect ratio channels, in particular, have larger surface-to-area ratios. This can facilitate higher flow boiling heat dissipation. However, because of bubbles and vapour slug confinement, more severe flow instability can be prevalent resulting in flow reversals, significant temperature fluctuations and a higher tendency for local dry-out [34,35]. Several methods have been considered to help mitigate such challenges with varying success. At low mass fluxes flow instabilities can become more pronounced due to rapid bubble growth. It is in these flow scenarios where self-rewetting of the heat transfer surface can reduce the adverse effects of flow instability by drawing liquid towards local hot spots.

To help address this, this investigation considered six fluids/mixtures: two self-rewetting (aqueous-alcohol solutions) and four non-self-rewetting mixtures. The aim is to perform direct comparison, specifically for a high-aspect ratio channel geometry with one-sided heating only. Besides the additional experimental data that is produced, the novelty of the study is the direct linkage with flow visualisation to illustrate how self-rewetting influences the flow patterns, heat transfer performance trends and occurrence of dry-out at low mass flux conditions. The selected aqueous-alcohol solutions provide a means of not only comparing self-rewetting and non-self-rewetting fluids but also two different concentrations of self-rewetting fluids.

Table 1
Some selected research studies conducted with different working fluids.

Authors	Conditions	Summary of findings
Vasileiadou et al. [28]	Water, ethanol, 5 % v/v ethanol-water mixture, 5 mm square channel, vertical upward flow, 0.33, 0.66, 1 kg/m^{2}s, uniform heating, range of heat fluxes	The binary mixture exhibited smaller wall temperature fluctuations than the pure substances. The study concluded that the binary mixtures allowed a more stable heat transfer process and could help in the prevention of wall dry-out during flow boiling.
Tsou et al. [29]	Water, ethanol, 0.1 – 0.89 molar fraction ethanol-water mixtures, diverging microchannel, horizontal flow, 175 – 700 kg/m^{2}s, non-uniform heating, range of heat fluxes	Convective boiling heat transfer and critical heat flux in a diverging microchannel with artificial cavities were considered. The critical heat flux increased for mixtures with molar fractions between 0 and 0.1 where after it decreased rapidly. The maximum critical heat flux was reached at a molar fraction of 0.1 which indicates that small additions of ethanol could result in better heat transfer capabilities.
Kuramae and Suzuki [30]	Water, 0 – 85 mol % ethanol-water mixtures, microgravity, horizontal flow, 10 mm circular tubes, uniform heating, $\dot{Q} = 100$ W	Thermal management solutions for space environments were considered. It was found that the addition of organic fluid can prevent the dry-out phenomenon and enhance heat transfer capabilities.
Abe, et al. [19]	Water, 1.5% wt/wt 1-butanol-water self-rewetting fluid, 25 % wt/wt ethanol-water mixture, microgravity, horizontal flow, 10 mm circular tubes, uniform heating, range of heat fluxes	For self-rewetting fluids, the Marangoni flow caused by concentration gradients coupled with thermocapillary flow induced strong liquid inflow at the three-phase interline of the bubble and heater contact area. This resulted in spontaneous liquid supply to local dry patches. For binary mixtures, only the concentration gradients contributed to liquid return. The self-rewetting fluid outperformed the binary mixture due to the latter reaching a dry-out limit at considerably lower heat fluxes.
Namura, et al. [21]	Water, 0.1 – 6 % wt/wt 1-butanol-water self-rewetting fluids, 1 - 2 % wt/wt ethanol-water mixtures, 50 μm chamber, horizontal flow, local heating, range of heat fluxes	The locally heated bubble flow along a surface was analysed. Transition concentrations were specified and were increasing for alcohols with a lower carbon number. For concentrations below the transition concentration, the fluid was driven from hot to cold regions. However, for concentrations above the transition value, the fluid was driven from cold to hot regions.
Sitar and Golobic [20]	Water, 1-butanol, 2 – 6 % wt/wt 1-butanol-water self-rewetting fluids, 25 μm and 50 μm square channels, horizontal flow, 83 – 208 kg/m^{2}s, non-uniform heating, 154 and 160 kW/m^2	Self-rewetting fluids demonstrated enhanced heat transfer coefficients compared to pure substances. High-speed visualization studies, contact angle measurements and surface roughness analysis indicated that the enhanced heat transfer was a result of improved wettability of the self-rewetting fluids. The self-rewetting property of the aqueous 1-butanol solutions

(*continued on next page*)

2. Experimental setup

2.1. Test facility

The experimental test facility which was also used in previous studies [28,36-46] is schematically represented in Fig. 2. The flow path assembly allowed for single-pass flow of a fluid through an electrically heated microchannel test section. Applicable sensors, data acquisition modules, and imagery equipment were installed within and around the test section to enable quantitative and qualitative data capturing.

The flow path included a syringe pump (item 1), an inlet test section interface assembly with pressure and temperature sensors (item 2), a transparent micro/mini test section with a layer of sputtered tantalum on one or both sides (item 3), an outlet test section interface assembly with pressure and temperature sensors (item 4) and a fluid collection reservoir (item 5). Other equipment included a backlight for test section

Table 1 (*continued*)

Authors	Conditions	Summary of findings
		stimulated annular flow and reduced maximum temperatures during microchannel flow boiling.
Shanahan and Sefiane [22]	5 % wt/wt 1-butanol-water self-rewetting fluid, 8 mm x 0.8 mm rectangular channel, horizontal flow, 1.5 ml/min, uniform heating, range of heat fluxes	Thermocapillary forces were demonstrated that could drive bubbles against the liquid flow. The unusual behaviour of migrating towards lower temperatures was ascribed to the non-linear surface tension temperature dependence. The bubbles settled at a stationary position downstream of the minimum surface tension. These trends were not seen for pure substances with linear surface tension profiles.
Mamalis et al. [18]	Water, 1-butanol, 5 % v/v 1-butanol-water self-rewetting fluid, 4 mm circular channel, Vertical upward flow, 0.2, 0.5, 1, 1.5 ml/min, uniform heating, range of heat fluxes	Bubble dynamics and thermocapillary stress development were considered. It was found that thermocapillary effects were prominent in the self-rewetting fluid, especially at lower volumetric flow rates. The thermocapillary effect was ascribed to the surface tension's quasi-parabolic temperature dependence. Enhanced heat transfer rates were reported for the self-rewetting fluids compared to pure substances.
Ono, et al. [31]	Water, 7.15 % wt ethanol-water mixture, 7.15 % wt/wt 1-butanol-water self-rewetting fluid, 1 mm circular channel, horizontal flow, 2.2 kg/m^{2}s, Uniform heating, Range of heat fluxes	The temperature-dependent surface tension profiles of the fluids were analysed by performing static maximum bubble pressure method tests. The measurements revealed the nonlinearity of the self-rewetting fluid's surface tension profile. The Marangoni effect was observed as the liquid layer extended to the hotter region. The liquid layer movement for the water-ethanol binary mixture was slower than that of the 1-butanol-water self-rewetting fluid.

illumination (item 6), a humidity meter (item 7), an infrared (IR) camera (item 8), and a high-speed (HS) visualisation camera (item 9). The flow path was located within an acrylic glass enclosure (1 m x 1 m x 1 m) to shield the experimental process from possible thermal fluctuations in the laboratory. Two computers (items 10 and 11) were situated outside of the acrylic glass enclosure and were used to capture the IR and HS camera imagery, whilst the second computer was used to capture the pressure transducer and thermocouple data. Lastly, a direct current (DC) power supply (item 12) was used to electrically heat the tantalum-sputtered test section, and was located outside of the acrylic glass enclosure.

Degassed liquid was pushed through the flow path with a factory-calibrated Cole Parmer 110 single-syringe infusion/extraction piston pump (item 1). A 50 ml Fortuna Optima glass syringe with an internal diameter of 26.96 mm (± 0.02 mm) was tightly fastened to the syringe pump. The piston was moved via a screw-thread mechanism connected to an electric motor with an adjustable speed which could ensure constant volumetric flow rates between 0.09 μl/min and 90.84 ml/min with a 99 % accuracy.

The inlet (item 2) and outlet (item 4) interface assemblies shown in Fig. 3a, were identical to each other and each contained a mounting block, L-type, and T-type push-pull PEM0310W John Guest® fittings, an Omega®PXM219 gauge pressure transducer, and K-type thermocouples. The end tubing used between the test section interface components and test section was rigid with an internal diameter and length of 4.5 mm and 20 mm, respectively. Thread tape was used to ensure air-tight connections. The test section interface mounting blocks were bolted onto an aluminium frame that was fixed to an electrically grounded side-mounted Axminster® rotary table. This allowed the channel inclination to be adjusted with an accuracy of ± 1°

The pressure transducers represented by P_1 and P_2 in Fig. 3a was connected to the flow path via the T-type fittings. They had a response time of approximately 2 ms and a measuring range of 0 to 250 kPa, with an accuracy of 0.025 % of the full-scale reading. Lastly, four K-type thermocouples indicated by T_1, T_2, T_5 and T_6 in Fig. 3a, each with a measuring tip size of approximately 1 mm were installed within each of the test section interface assemblies (two thermocouples in each). The thermocouples were inserted directly into the fluid by passing through small holes that were drilled into the l-type and T-type fittings.

The test section (item 3) which is fully described in Section 2.2 and showed in Fig. 3, was used to heat the fluid. It consisted of an extruded rectangular borosilicate glass channel with a glass-blown end cap on each side. The channel was sputtered with a thin, uniform, transparent, metallic deposit of tantalum on one or both exterior walls. Aluminium foil strips were placed at the microchannel outer edges to act as electric terminals. Clamps were used to connect the microchannel terminals to the DC rectifier, creating a closed electrical circuit. In addition to the thermocouples in the inlet and outlet assemblies, each end cap had a small glass-blown hole to allow the insertion of another K-type thermocouple as indicated by T_3 and T_4 in Fig. 3a close to the channel inlet and outlet, respectively. This amounted to a total of six thermocouples (three at the inlet and outlet, respectively) to improve the accuracy of the temperature readings. All six thermocouples were sealed and fixed in place with Dowsil®−732 multi-purpose sealant and Araldite® Rapid epoxy. The sealant is non-reactive and dielectric with a melting temperature of 180 °C, well above the boiling temperature of all working fluids used in this study. The epoxy was applied over the sealant to increase the rigidity of the connection and special care was taken to ensure that it did not come into contact with the fluid as it had a melting temperature of 80 °C. The epoxy's melting temperature was below the boiling temperature of some of the working fluids used during this study, which could lead to contamination, explaining the need for the sealant with a much higher melting temperature.

Flexible hosing with a 6 mm internal diameter and an accumulative length of 1.4 m was used to connect the syringe pump and inlet interface as well as the outlet interface and glass reservoir. The tubing, hosing and reservoir were not thermally insulated, resulting in condensation, and cooling of the test fluid once it had passed through the test section. The reservoir was fitted with both a drainage pipe, to recover the used working fluid, and a vent to the outside of the laboratory to maintain the system at an atmospheric pressure of approximately 101 kPa.

The experimental setup enabled simultaneous wall temperature acquisition and flow visualisation in the test section. The local external test section heated (via the tantalum) wall temperature was recorded with a FLIR® A645 IR camera (item 8) with a resolution of 640 × 480 pixels, a thermal sensitivity of 20 mK, a maximum frame rate of 25 frames per second (fps) and an upper-temperature measurement limitation of 150 °C. The IR camera was fixed at a constant measuring distance from the test section. Furthermore, it was orientated at a slight orthogonal offset of approximately 5° relative to the heated test section surface to prevent self-reflection aberrations which would result in inaccuracies in the wall temperature readings.

Flow visualisation was achieved via a Basler® acA800–510um CCD high-speed camera (item 9) with a 12 mm fixed lens, a maximum frame rate of 511 fps and a resolution of 800 × 600 pixels. The camera was used to record the flow boiling process seen inside the test section. A backlight (item 6) was situated at the opposite side of the channel for

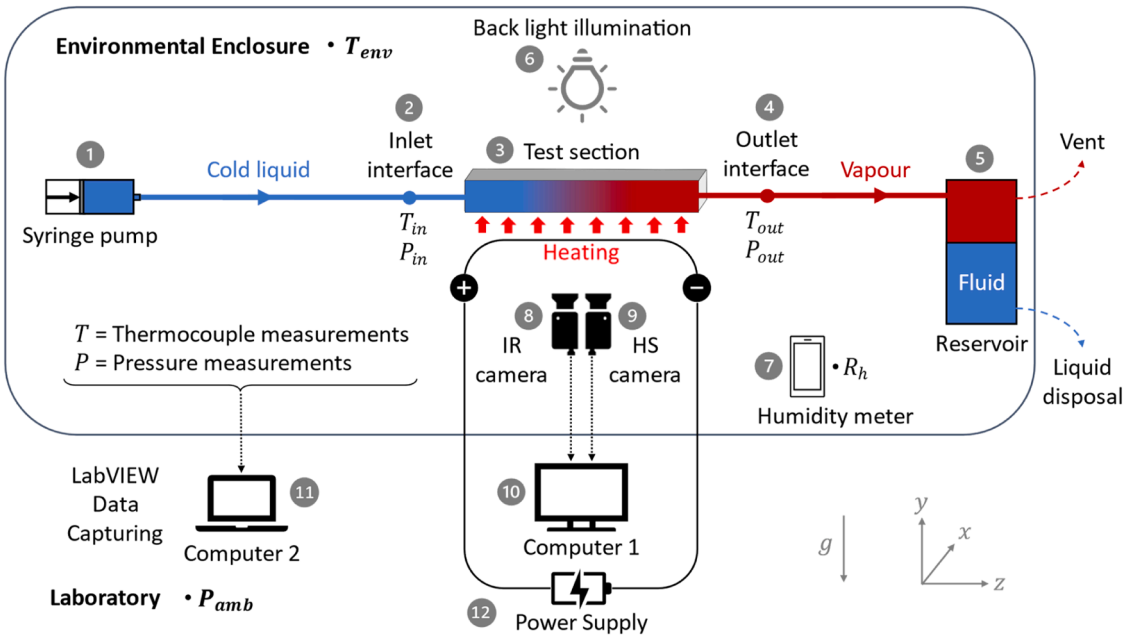

Fig. 2. Experimental test facility schematic.

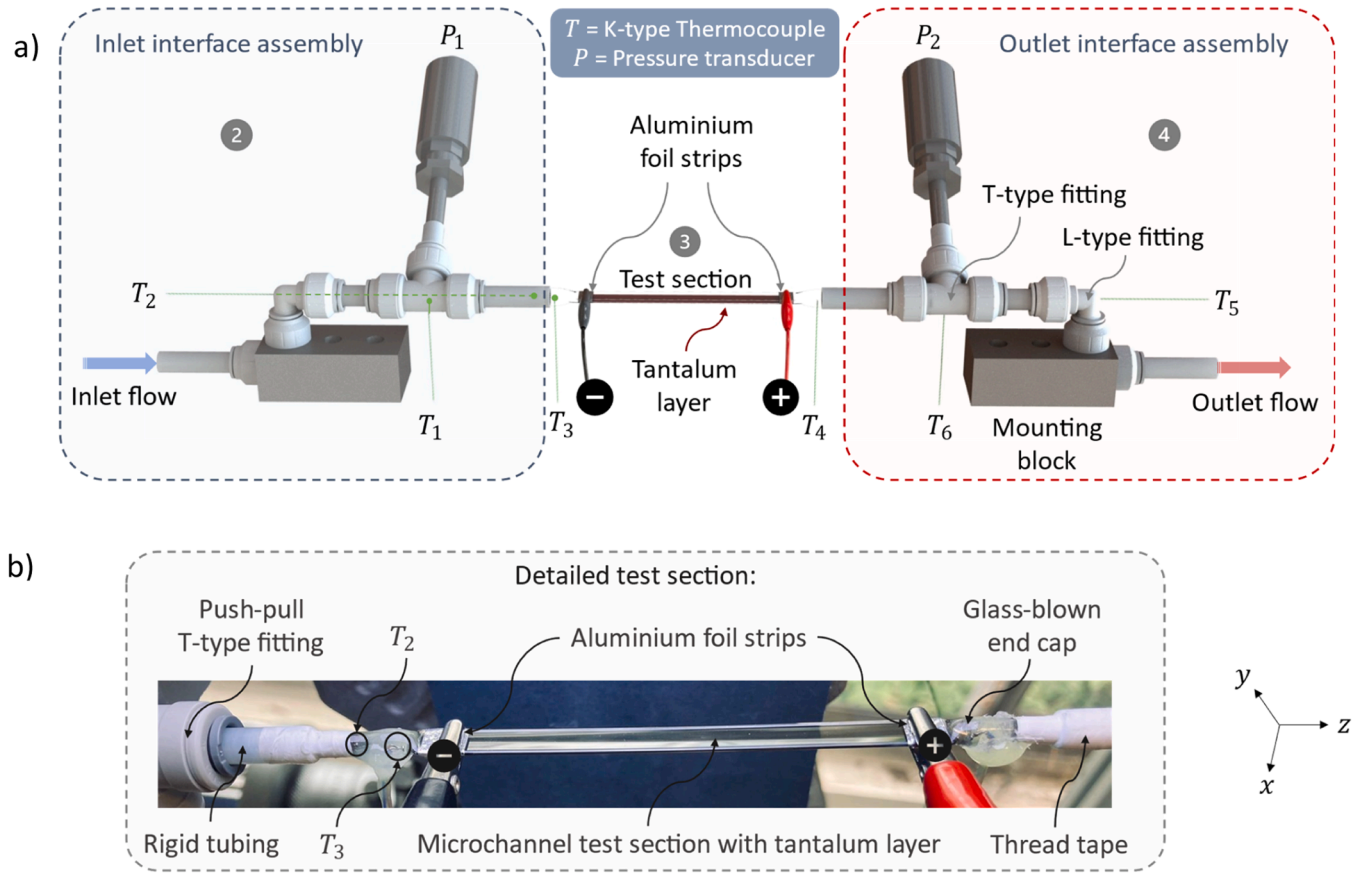

Fig. 3. a) Test section interface assembly schematic, thermocouple placement, and b) detailed test section image.

illumination purposes. As previously mentioned, the entire flow path, as well as both cameras, were all enclosed in an acrylic glass container. The internal enclosure environmental temperature and humidity were respectively monitored and recorded by two K-type thermocouples (T_7 and T_8) and an Omegaette® HH311 Series humidity meter (item 7) with an accuracy of 2.5 %.

Electrical heating was supplied to the microchannel test section by a power supply (item 12) which consisted of a dial-operated Clairtronic® 240 V, alternating current (AC) VARIAC transformer, connected to a direct current (DC) rectifier. A Kethley 192 programmable digital

multimeter was connected in parallel with the circuit to measure the applied voltage with an accuracy of 0.011 % + 1 V. A Kethley 175 Autoranging digital multimeter was connected in series with the circuit to measure the current in mA with an accuracy of 0.2 % + 2 mA.

ResearchIR software was used as the IR camera interface to visualise and record the heated microchannel surface temperatures in the form of a video. Later, each pixelated frame in the video was exported as MATLAB matrices for data handling purposes. Before data exporting, the software required several input settings to be specified, these included the atmospheric temperature, reflected temperature, optics temperature, humidity, camera distance from the heated microchannel and the microchannel surface emissivity. Basler AG's Pylon Viewer software was used to visualise and record high-speed camera images.

The eight K-type thermocouples were attached to a National Instrument® (NI) SCX1–1303 data card, which was slotted into a NI SCXI-100 chassis. The two pressure transducers were attached to an NI USB-6008 stand-alone data acquisition unit which had a time delay of approximately 200 μs for readings obtained from the different channels. Both the temperature and pressure data were sampled at 100 Hz.

2.2. Test section

Fig. 4 gives an overview of a typical test section which consisted of a rectangular borosilicate glass channel and two hollow borosilicate glass end caps (Fig. 4a) which were bonded via a glassblowing process. Due to the microchannels being very fragile and prone to breakage, a set of twelve identical microchannels was acquired from VirtoCom™. The microchannels had an axial length (L) of 75 to 80 mm ± 0.02 mm in the z-direction (Fig. 4b), an inner width (W) of 6 mm ± 0.02 mm in the x-direction and an inner depth (H) of 0.3 mm ± 0.02 mm in the y-direction (Fig. 4c). The channel had a wall thickness (t_w) of 0.3 mm ± 0.02 mm, which was uniform along the length of the microchannel (Fig. 4c). Each end cap which had a diameter of 4 mm ± 0.02 mm.

The microchannels were thoroughly cleaned whereupon tantalum was sputtered on all the microchannels in a class ten cleanroom at the Scottish Microelectronics Center (SMC). The applied tantalum layer thickness was measured with a nanoscope and showed to be approximately 11 nm and transparent. Depending on the required test cases, sputtering was done either on the bottom or both walls of the microchannels. Electronic connection with the tantalum was enabled via the aluminium foil (Fig. 4b). The heated length (L_h) was 65 to 70 mm ± 0.01 mm and had a surface resistivity of 120 Ω/m for single sided coatings.

The flow passage had a hydraulic diameter of 571.43 μm and an aspect ratio of 20. Due to the inconsistencies relating to microchannel classification, several dimensionless numbers were evaluated to verify whether micro-scale physics would be at play.

3. Experimental procedure

3.1. Equipment calibration

Devices that were specifically calibrated in detail included the syringe pump settings, thermocouples and data acquisition system, pressure transducers and the IR camera settings. Although the syringe pump was factory-calibrated, a custom syringe specification of 26.96 mm internal diameter was used. The thermocouples were calibrated with a Julabo® F25-MC thermal water bath which had a temperature measurement resolution of 0.01 °C. Twelve calibration temperatures were considered from which eight thermocouple-specific linear correction correlations were derived, reducing the measurement error to ± 0.15 °C. The pressure transducers were calibrated with a SPER SCEINEFITIC® Model 84,083 manometer with a measurement uncertainty of ± 0.3 %. Twenty-four pressure readings were considered from which pressure transducer linear correction correlations were derived, reducing the measurement error to ± 126 Pa.

The Tantalum-sputtered surface emissivity was unknown due to the custom manufacturing process and had to be determined using comparative correlations [47] using a matt black painted reference body with a known emissivity value of 0.97 [48]. Calibrated thermocouples were used to measure the external test section wall temperature at 3 different locations for six controlled steady-state temperature conditions ranging between 22 °C and 55 °C. The tests were done both with the reference black painted and tantalum-sputtered microchannels. The implementation of the comparative correlations rendered an average

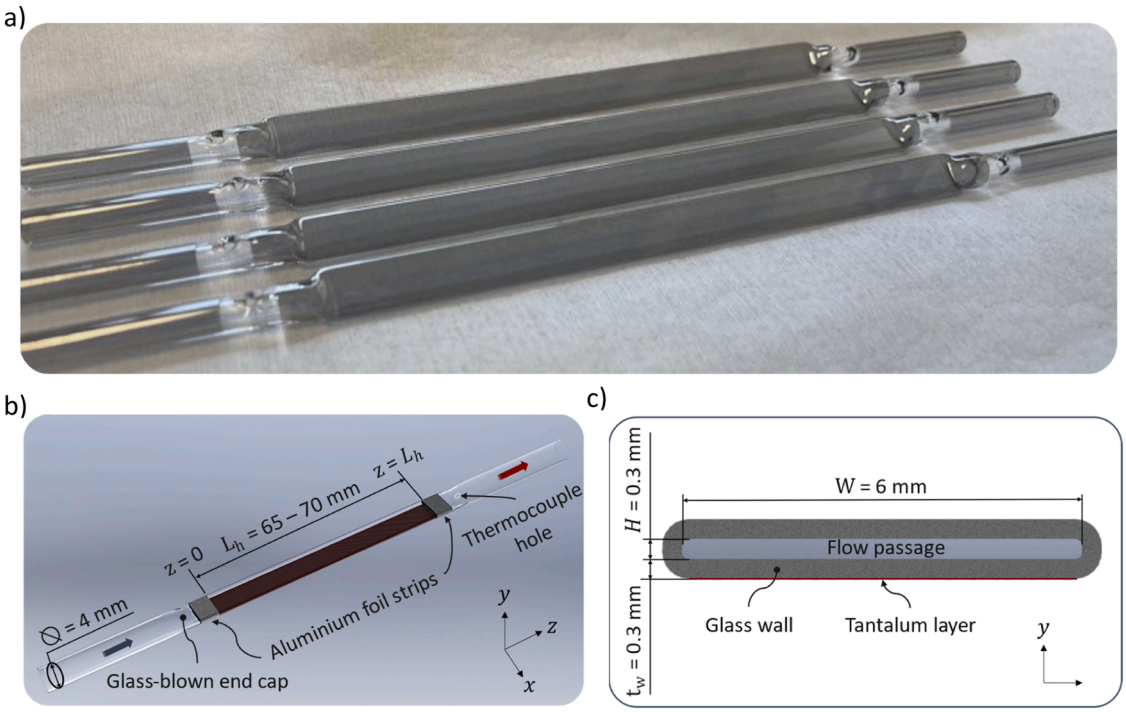

Fig. 4. a) Image of the manufactured test section and schematics illustrating the b) microchannel isometric and c) cross-sectional views.

Tantalum-sputtered channel surface emissivity of 0.79 which agreed with similar research studies [18,36,37,39,40,42-44,46]. The average wall temperature measurement error was reduced from ± 2.2 °C to ± 0.15 °C, yielding an absolute uncertainty of ± 0.48 °C.

3.2. Experimental test matrix

This experimental study aimed to investigate the influence that the working fluid has on the heat transfer mechanisms during microchannel flow boiling. Six different test fluids were used during the investigation of which three were pure substances (water, ethanol, and 1-butanol) and three were dilute aqueous solutions (5 % v/v ethanol-water, 5 % v/v 1-butanol-water and 7 % v/v 1-butanol-water). Special attention was given to how the dilute water-alcohol solutions' heat transfer performance compared to that of their pure substance counterparts.

A previous study reported that low mass fluxes result in buoyancy effects becoming more prominent, which could lead to increased heat transfer performance [18]. Furthermore, in industrial applications, it is advantageous to have low mass flux requirements as this results in smaller pump size requirements. The three mass fluxes (G) selected for this experimental investigation included 10 , 15 and 25 kg/m^{2}s (± 0.08 kg/m^{2}s), corresponding to single-phase Reynolds numbers which ranged between 5 and 16 indicating laminar flow conditions.

The associative heat flux ranges were mass flux and working fluid specific. The heat flux ranges covered both single-phase liquid experiments and two-phase flow boiling cases. The single-phase liquid experiments were deemed necessary due to the constraint of not being able to thermally insulate the test section without hindering flow visualisation studies. Without thermal insulation, substantial heat loss occurred from the heated tantalum surface to the surrounding atmosphere. It was crucial to evaluate the heat loss to accurately determine the heat transferred into the fluid, which was required to determine the local and average heat transfer coefficients. The heat loss evaluation was performed during the steady-state, single-phase, liquid experiments whilst up to fifteen heat fluxes were considered per working fluid and mass flux.

The lowest two-phase heat flux input was selected at the onset of nucleate boiling (ONB) whilst ensuring that the quasi-steady-state outlet thermocouple temperature measurement was approximately at the working fluid's saturation temperature (T_{sat}). This was done to ensure no subcooled boiling cases were included in the test matrix, but rather only saturated boiling cases. Subcooled boiling occurs when boiling initiates whilst the bulk liquid temperature remains below the saturation temperature and is notoriously known to happen in confined test sections with a high aspect ratio. The highest two-phase heat flux input was limited either by the IR camera temperature measurement limitation of 150 °C or when it was evident that almost the entire interior of the channel was vaporised, risking burn-out of the tantalum layer. It should be noted that the IR camera temperature measurement limitation was found to mostly govern the final heat flux input due to some of the selected working fluids having relatively high saturation temperatures. Table 2 provides a breakdown of the experimental test matrix considered in this paper.

The measured mixture saturation temperatures were found to be similar to those reported by previous researchers [20,21,28] and were thus accepted to be correct. The average environmental temperature (T_0) in the lab was 24 °C ± 3 °C, which dictated the inlet temperature ($T_{in} \approx T_0$) while the pressure was 101.1 kPa. Depending on the fluid, the degree of inlet liquid subcooling was between 54 °C and 93 °C.

The effect of inlet fluid subcooling on microchannel flow boiling depends on the specific conditions of the system, including the channel geometry, working fluid properties, and applied heat flux range. It has been shown that the degree of inlet liquid subcooling influences the flow pattern development and transition causing differences in the total pressure drop, heat transfer coefficients, critical heat flux and void fraction [49,50]. In addition, researchers discovered that the impact of subcooling on the heat transfer coefficients was magnified at degrees of subcooling of 20 °C or lower, whilst there was little effect on the heat transfer coefficients at subcooling levels above 25 °C [49-51]. Thus, although variability in the level of subcooling was evident during this experimental investigation, it was accepted that the effect would be minimal.

Table 2
Experimental test matrix for data contained in this paper.

Working fluid	Saturation temperature T_{sat}, °C	Mass flux G, kg/m^{2}s	Effective heat flux $\dot{q}$, kW/m^2	
			Single phase runs	Flow boiling region
Pure Water	99.74 ± 0.1	15	0.3 – 13.5	21.1 – 25.9
		25	0.6 – 16.8	36.5 – 41.6
Pure Ethanol	78.34 ± 0.1	10	0.4 – 8.9	6.7 – 13.2
		15	0.5 – 11.7	10.1 – 22.6
		25	0.7 – 19.6	14.2 – 34.6
Pure 1-Butanol	116.58 ± 0.1	15	0.4 – 10.8	15.3 – 20.8
5 % v/v 1-Butanol-Water	93.5 ± 0.1	10	0.9 – 12.4	11.7 – 20.0
		15	0.3 – 15.2	24.2 – 31.3
		25	0.9 – 27.9	46.9 – 53.1
7 % v/v 1-Butanol-Water	92.2 ± 0.1	10	0.8 – 12.8	13.1 – 19.9
		15	0.3 – 17.7	25.6 – 29.6
		25	1.0 – 31.9	41.0 – 51.4
5 % v/v Ethanol-Water	93.9 ± 0.1	10	0.3 – 6.6	8.4 – 16.7
		15	1.2 – 11.3	14.0 – 28.1
		25	1.2 – 14.9	23.2 – 47.0

3.3. Experimental method

3.3.1. Working fluid and system preparation

The working fluids and experimental flow path were prepared before each main set of experiments. The working fluid preparation consisted of water degassing and mixture formulation. The working fluids were prepared daily before the experiments were initiated to ensure consistency. Before each main set of experiments was performed with each of the considered working fluids, the entire flow path was flushed several times. First, deionised water and thereafter, the selected working fluid was pushed manually through the flow path at a high volumetric flow rate and different inclinations to ensure that all impurities and air/vapour bubbles were removed. It should be noted that the alcohols used during this investigation, were soluble and miscible in water, eliminating the need to air-dry the flow path between flushing with pure water and the respective working fluids. Furthermore, the working fluids were also tested in such an order to minimise the probability of contamination.

Once the flow path was prepared with the selected working fluid and visually inspected to be according to standard, the syringe was refilled with the selected working fluid, the rotary table was adjusted and fixed at a horizontal orientation and the rest of the system was prepared. This involved opening and running the respective software programs and testing the validity of the displayed measurements.

3.3.2. Single-phase heat loss characterisation experiments

As mentioned previously, thermal insulation of the test section was not possible without restricting flow boiling visualisation. Due to the intentional absence of channel insulation, substantial heat loss occurred from the heated tantalum surface to the atmosphere within the acrylic glass container. When considering the energy balance of the system, the total power input should equal the sum of the heat lost to the environment and the heat absorbed by the fluid. Whilst both of the latter were unknown, the heat transfer rate into the fluid was essential to calculate the local and average heat transfer coefficients. Due to flow boiling exhibiting chaotic characteristics, it was challenging to accurately determine the thermodynamic states of the fluid based on the inlet and

outlet temperature and pressure measurements. This made it inviable to directly calculate the heat transfer rate into the fluid, highlighting the importance of characterising the heat lost to the environment correctly.

Steady-state single-phase liquid experiments enabled the direct measurement of all required variables to calculate the heat absorbed by the fluid. These variables included the total power input, steady inlet and outlet fluid temperatures, the environmental temperature, and the heated Tantalum surface temperature. Such single-phase steady-state liquid experiments, or void methods (where the channel is dry), over a range of heat fluxes, which enables the characterisation of fluid-specific heat loss rate functions, are techniques that have been used by multiple previous researchers [32,42,52-56]. Because this study considered single-sided heating, a wet method whereby a fluid is present inside the channel was opted for to better represent the thermal scenario during the flow boiling conditions.

The applied heat flux range varied for all cases, with the highest applied heat flux being before boiling incipience, was induced. Between 10 and 20 single-phase liquid experiments were conducted for each mass flux and working fluid combination to ensure a high-resolution and representative heat loss function could be obtained. For each heat input case, a steady state approach was adopted by ensuring that the outlet fluid temperature readings changed by <0.1 °C for 3 minutes. After steady-state conditions were reached, data logging and recording were done for 30 seconds. The used fluid collected in the outlet reservoir was not reused, but retrieved and stored in a sealed container until it could be disposed of safely.

3.4. Two-phase flow boiling experiments

After the completion of the steady-state single-phase liquid experiments for the selected mass flux and working fluid, the main two-phase flow boiling experiments were conducted. The lowest heat flux input for the two-phase flow boiling experiments was selected based on visual boiling incipience being achieved and the outlet thermocouples measuring a constant saturation temperature; thus, only saturated flow boiling cases at quasi-steady-state conditions were considered. The power supply was gradually increased to the desired value to prevent any sudden or unwanted system instabilities.

Once quasi-steady-state flow boiling conditions were achieved, 60 seconds was provided after which data acquisition was started. The pressure and thermocouple measurement data were logged for 65 seconds at 100 Hz, whilst the IR camera surface temperature and HS camera footage were recorded for 60 seconds at 25 fps and 511 fps, respectively. Each working fluid test case (mass and heat flux combination) was repeated three times after which the next increased heat input test case could be considered. Between eight and twelve different heat flux input test cases were completed for each of the working fluid and mass flux combinations. The highest heat input case was governed by either the IR camera surface temperature measurement limitation of 150 °C or when almost the entire channel was filled with vapour, posing the risk of damage or burn-out of the Tantalum layer. After each set of experiments, the condensed fluid collected in the outlet reservoir was retrieved and stored in a sealed container until it could be disposed of safely.

4. Data reduction

Due to the lack of a sufficient fluid property database for the specified ethanol-water and 1-butanol-water mixture compositions, the thermophysical properties of the three mixtures were approximated by applying the linear ideal mixing rule. This simple mixing rule is based on the first law of thermodynamics and holds for mixing that is neither endo- nor exothermic [57]. The properties approximated by the simple mixing rule included the fluid's density (ρ), specific heat capacity (C_p) and enthalpy (h) which were evaluated over a range of temperatures towards obtaining temperature-dependent polynomial functions. The solute was the minor component in the mixture (ethanol or 1-butanol) and the solvent was the major component into which the solute was mixed (pure water).

The approximated mixture property (γ_{mix}) was obtained by considering the respective molar fractions (η_i and η_{ii} for solute and solvent respectively) and the accompanying pure substance's property at the specific temperature (T) and pressure (P):

$$\gamma_{mix}(T,\ P) = \eta_i\gamma_i(T,\ P) + \eta_{ii}\gamma_{ii}(T,\ P) \tag{1}$$

Notably, this is a conservative approach as opposed to when the Gibbs energy of mixing is considered. Raoult's law is applied quantitively for solutions in which the molecules of the components are similar in size, shape, and intermolecular forces. For diluted solutions with low concentrations of solute, Henry's law can be considered for application. For both approaches, partial molar properties are applied [58]. However, even with these involved approaches, the mixtures are assumed to be ideal and are purely statistical, deviating from real mixtures' chemical behaviour [59].

Due to each mixture being distinct in composition, researchers have ventured into developing empirical correlations to capture mixture properties. Although some researchers have claimed success in developing such correlations for ethanol-water mixtures, the mixture compositions are limited [60] and little experimental data was used for validation [61]. Due to 1-butanol-water mixtures being an uncommon mixture that has not been investigated thoroughly, empirical correlations could not be found. Furthermore, researchers found that the uncertainties increased within the two-phase region. Considering these facts and wanting to stay consistent during the evaluation of this research study's experimental data, the conservative approach of applying the simple mixing rule (Eq. (1)) was favoured.

During the single-phase flow cases, the rate of heat loss from the Tantalum surface ($\dot{Q}_{loss}$) was calculated by comparing the power supply input rate ($\dot{Q}_{input}$) and the rate of heat absorbed by the liquid ($\dot{Q}$):

$$\dot{Q}_{loss} = \dot{Q}_{input} - \dot{Q} \tag{2}$$

The heat power input rate to the test section was calculated by considering the measured DC voltage (U) and current (I) at the power supply unit as well as the wiring resistance (R_{wire}) between the power supply unit and the test section:

$$\dot{Q}_{input} = I^2\left(\frac{U}{I} - R_{wire}\right) \tag{3}$$

The heat transfer rate to the liquid was determined from:

$$\dot{Q} = \dot{m}C_p(T_{out} - T_{in}) \tag{4}$$

Here T_{in} and T_{out} are the time-averaged inlet and outlet fluid temperatures measured by thermocouples T_1, T_2 and T_3 at the inlet and T_4, T_5, and T_6 at the outlet of the microchannel. The specific heat capacity (C_p) was taken at the bulk fluid temperature whilst the constant mass flow rate ($\dot{m}$) was determined from the syringe pump volumetric flow rate ($\dot{V}$) and the liquid density (ρ_l):

$$\dot{m} = \dot{V}\rho_l \tag{5}$$

For the mixtures, Eq. (1) was used to determine C_p and ρ_l, while for the pure substances, Coolprop was used.

The heat loss rates obtained from Eq. (2) were correlated to the spatially averaged temperature difference between the heated Tantalum surface ($\overline{T}_s$) obtained from the IR camera, and the surrounding enclosure temperature (T_0) obtained from averaging thermocouples T_7 and T_8. A linear mathematical fit of the following format was found to describe most of the single-phase data points:

$$\dot{Q}_{loss} = f(\Delta T_s) \text{ with } \Delta T_s = \overline{T}_s - T_0 \tag{6}$$

Similar methods were applied by previous researchers [32,42,52-56]. Fig. 5 provides the heat loss characterisation for sample sets for

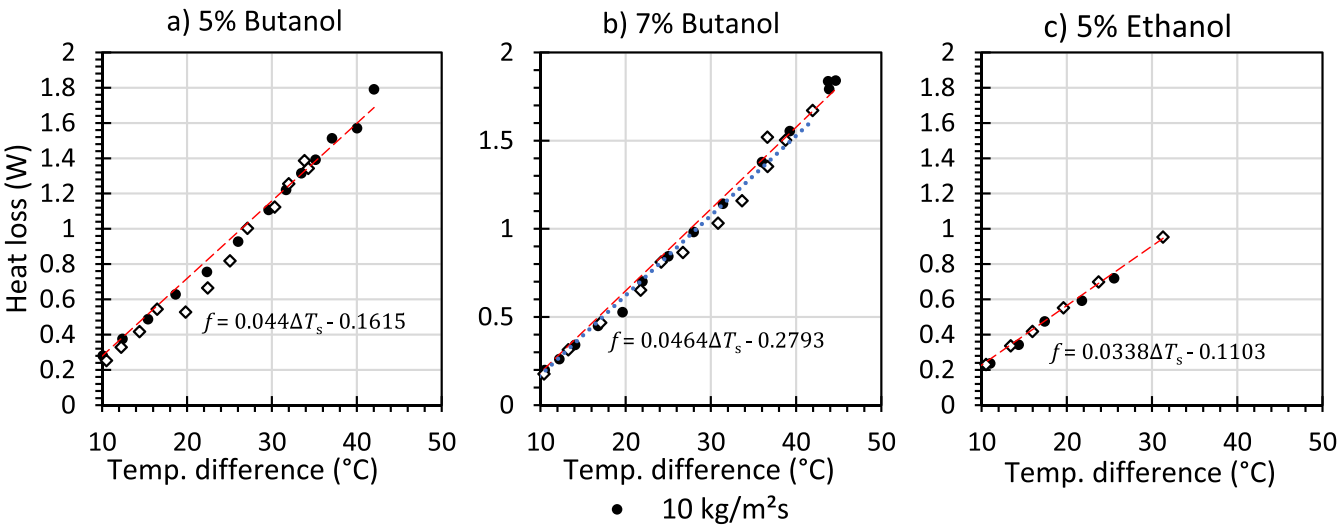

Fig. 5. Heat loss characterisations for the a) 5 % Butanol mixture, b) 7 % Butanol mixture and c) 5 % Ethanol mixture at 10 and 15 kg/m^{2}s.

the fluid mixtures at 10 and 15 kg/m^{2}s. Even though similar characteristics were observed for all fluids, custom constructed functions f were implemented for each fluid type and mass flux operating condition. Even though the test section was inside a shielded enclosure, recalibration was performed daily and applied to the relevant flow boiling data sets. For the data included in Fig. 5, linear heat loss trends resulted in the best data fit, and had coefficients of determination (R^2) greater than 0.99. As can be seen, the heat loss rate increased with temperature difference. The heat loss functions predicted the heat loss rate values with a maximum error of ± 0.09 W, whilst the absolute error for the temperature differences was found to be ± 0.52 °C.

The heat loss was rewritten as a heat loss flux by dividing the heat loss rate by the heated surface area, $A_h = L_h(W + H)$, as follows:

$$\dot{q}_{loss}(z) = \frac{\dot{Q}_{loss}}{A_h} = \frac{f(\Delta T_s(z))}{L_h(W+H)} \tag{7}$$

It was approximated that due to in-wall conduction only half of each of the vertical walls contributed to the inner surface heat transfer rate. The local heat loss along the length of the test section (z-direction) was determined by using the width-wise time-averaged tantalum surface temperature, $T_s(z)$, which was obtained from the IR camera measurements. A spatial resolution that matched to the pixel size of the IR camera (approximately $\Delta z = 0.2$ mm) was used.

For the two-phase flow boiling experiments, the local effective heat flux was determined as follows:

$$\dot{q}(z) = \frac{\dot{Q}_{input}}{A_h} - \dot{q}_{loss}(z) \tag{8}$$

Here, $\dot{Q}_{input}$ was computed with Eq. (3) and based on single-phase calibration to account for any local variation.

The local bulk fluid temperatures (T_f) was calculated via the energy balance principle applied to subsequent control volume divisions:

$$\text{If } T_f(z) < T_{sat}: \; T_f(z) = T_f^n = T_f^{n-1} + \frac{\Delta z(W+H)\dot{q}(z)}{\dot{m}C_p} \tag{9}$$

$$\text{else}: T_f(z) = T_{sat} \tag{10}$$

Here superscripts n and $n-1$ refer to a relevant control volume and its upstream neighbour respectively and $z = n\Delta z$. The inlet is at $n = 0$ ($z = 0$) such that $T_f = T_{in}$. The specific heat capacity, C_p and other relevant fluid properties were re-evaluated at each control volume based on the upstream fluid temperature using Coolprop and the derived mixing rule formulation of Eq. (1).

The local bulk vapour quality (χ) was numerically calculated by considering the specific enthalpy (h), the fluid's saturated liquid specific enthalpy (h_f) and specific latent heat of evaporation (h_{fg}):

$$\chi(z) = \frac{h(z) - h_f}{h_{fg}} \tag{11}$$

where

$$h(z) = h_{in} + \frac{(W+H)}{\dot{m}} \int_0^z \dot{q}(z)dz \tag{12}$$

$$h_f = h_{in} + \int_{T_{in}}^{T_{sat}} C_p(T_f)dT_f \tag{13}$$

Due to the subcooled nature of the fluid entering the channel, negative vapour qualities were realised within the single-phase region and indicated the measure of liquid subcooling. The local vapour qualities within the two-phase region yielded positive values between 0 and 1.

From the local effective heat flux and the local bulk fluid temperatures the local heat transfer coefficients based on the outer glass temperature (α_0) and inner glass temperature (α) was calculated by Eqs. (14) and (15) respectively:

$$\alpha_0(z) = \frac{\dot{q}(z)}{T_s(z) - T_f(z)} \tag{14}$$

$$\alpha(z) = \frac{\dot{q}(z)}{T_s(z) - \frac{\dot{q}(z)t_w}{k_w} - T_f(z)} \tag{15}$$

Eqs. (14) thus includes conduction effect in the glass wall, as well as the inner surface heat transfer coefficient while in Eq. (15) the wall temperature difference is removed first. The thermal conductivity (k_w) for the borosilicate glass channel was 1.14 W/mK.

Average reported flow boiling heat transfer coefficients in the result sections were obtained by using the spatially averaged IR surface temperature downstream from the bulk saturated liquid point ($\chi \geq 0$) excluding the dry-out region and/or the last 5 mm of the test section to avoid any influences that might have been caused by edge effects. Lower heat flux cases where flow boiling only initiated towards the end of the channel is thus not included in the result section.

5. Uncertainty propagation analysis

Absolute uncertainties were used for constant parameters (independent of measurement scale), whilst relative uncertainties were implemented for parameters that were dependent on multiple variables. A full description of uncertainty propagation is contained in reference [62]. Table 3 provides a breakdown of the mean absolute and relative uncertainties calculated for each of the important parameters.

6. Discussion of results

6.1. Validation

The validity of the experimental setup, test procedure and data analysis methods were checked by comparing results with a published study where a similar experimental setup and procedure was used [46]. Although this study predominantly focused on one-sided (locally uniform) heating, the validation case was performed with uniform two-sided heating to align with the reference study. Perfluorohexane, a Fluorinert™ Electronic Liquid (FC-72), was used as the test fluid due to its availability within the lab and its usage during the reference study.

The published study [46] was mimicked by performing experiments with a horizontally-mounted microchannel of the same geometry, using FC-72 as the working fluid, a mass flux of 44.8 kg/m^{2}s and including a range of uniformly applied heat fluxes. Single-phase and two-phase flow boiling experiments were performed to validate the experimental setup, procedure, and data-handling approach. The validation study was performed by following the experimental procedure, data handling approach and analysis methods as described in Sections 3 and 4, respectively.

Fig. 6 presents a comparison of the published average heat transfer coefficient results [46] (red) and those obtained during the validation study (blue). Error margins are included based on the uncertainty analysis for each of the studies.

The heat transfer coefficient calculation depends on multiple variables, making it a valuable parameter to consider during validation studies. As illustrated by the error margins included in the graph, this study's uncertainties (marked in red) were smaller than those reported by the previous study (marked in blue) [46]. The error margin difference can be ascribed to the errors and uncertainties found during equipment calibration. The uncertainties and errors found for this study (as summarised in Table 3), were smaller than those documented during the previous study [46].

It is evident that the respective boiling curves had the same profile and agreed regarding the first flow boiling case at approximately 6.1 kW/m^2. Furthermore, the data produced by the validation study closely correlated with the reference data set by always falling within the uncertainty band for both the single-phase and two-phase experiments. Based on the agreement between these results, it was concluded that the experimental setup, procedure, and data reduction methods would produce accurate and repeatable results. It specifically illustrated that both the single-phase and two-phase flow boiling analysis were performed correctly, but also acted as reassurance towards the heat loss characterisation performed.

Table 3
Mean relative and absolute uncertainties for several parameters considered during this study.

Parameter/Quantity	Mean relative error	Mean absolute error
Input quantities:		
Channel dimensions (L, W, H)		± 0.02 mm
Heated length (L_h)		± 0.01 mm
Inlet temperature (T_{in})		± 0.12 °C
Environmental temperature (T_0)		± 0.14 °C
Outlet temperature (T_{out})		± 0.12 °C
Mass flux (G)	5.01 %	± 1.12 kg/(m^{2}s)
Voltage (U)	0.18 %	± 0.02 V
Electric current (I)	2.74 %	± 0.09 mA
Derived and calculated quantities:		
Heat input rate ($\dot{Q}_{input}$)	2.74 %	± 0.68 W
Local surface temperature (T_s)		± 0.48 °C
Heat loss rate ($\dot{Q}_{loss}$)	1.51 %	± 0.09 W
Effective heat flux ($\dot{q}$)	3.60 %	± 1.37 kW/m^2
Vapour Quality (χ)	4.34 %	0.005
Bulk fluid temperature (T_f)		4.67 °C
Average overall heat transfer coefficient (α_0)	5.87 %	137.04 W/m^{2}K
Average inner surface heat transfer coefficient (α)	8.13 %	

6.2. Local axial variations

Focussed was placed on both qualitatively examining the bubble dynamics and quantitatively analysing the heat transfer performance due to the concepts being interconnected. To illustrate this, and for the sake of brevity, an example test case with the 5 % v/v 1-butanol-water self-rewetting fluid is presented here. The selected example experimental test case was conducted at a mass flux of 10 kg/m^{2}s and an average effective heat flux of 14.76 kW/m^2.

Fig. 7 presents the acquired set of results showcasing the HS and IR camera footage as well as the locally calculated results over the test section length. The calculated results displayed include the local surface and fluid temperatures, effective heat flux, vapour quality and heat transfer coefficient.

As seen in Fig. 7b, bubble nucleation sites were present within the first quarter of the channel. Due to the continuous heat input, the bubbles would slowly grow in size and periodically detach from the nucleation sites. The inertial forces would result in the bubble being moved further along the channel length where the combination of continuous heat input and increased fluid temperatures resulted in further bubble growth. A vapour slug with entrailed liquid films existed at the channel outlet which saw periodic movement or fluctuations which triggered a type of churn flow.

As should be evident from Fig. 7a and further indicated in Fig. 7c, the realised flow patterns influenced the measured surface temperatures accordingly. Although not that visible at the bubble nucleation sites, it is specifically evident at the detached bubble and vapour slug locations which are situated at the channel heated lengths of approximately 36 mm and 54 mm to 70 mm, respectively. A further increase in the local surface temperature is visible at the channel outlet which indicates the occurrence of dry-out. Typically, liquid films existed around the vapour slug, however, at increased temperatures, the liquid film would also evaporate. The liquid film evaporation resulted in vapour being in direct contact with the channel's heated surface and caused dry-out. Dry-out degrades the heat transfer performance due to vapour having significantly lower heat absorption capabilities as opposed to liquid.

Fig. 7c also shows the calculated bulk fluid temperature along the channel length based on the local energy balance. Because this calculation method only desribes the thermodynamic bulk temperature, local fluid temperature variations at nucleation sites and within the vapour slug region can not be represented. The energy blance method can, however, serve to determine the portion of the channel that is at saturation, where the fluid temerature remains constant along the flow direction.

The local heat loss, and evidently the local effective heat flux, shown in Fig. 7d, was influences by the surface temperatures. The local

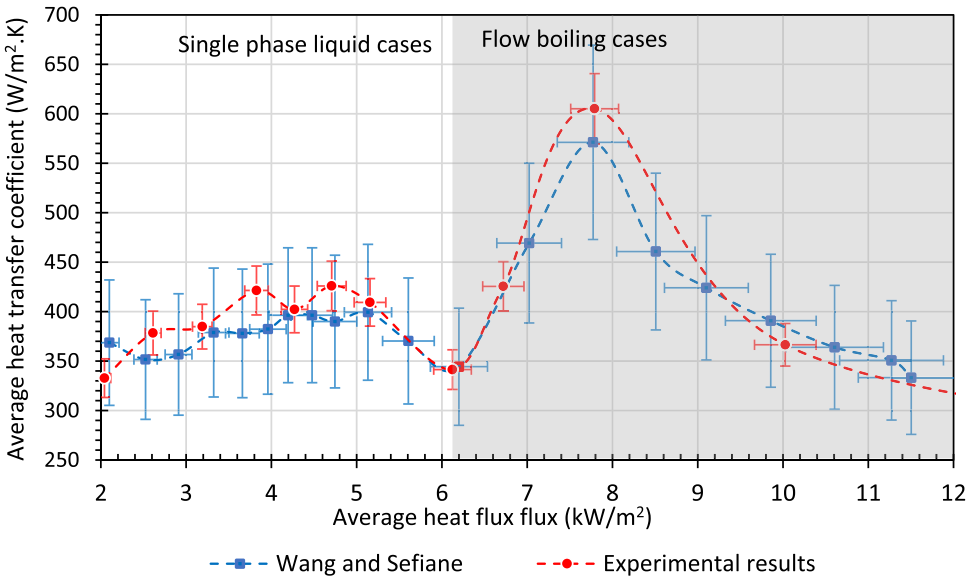

Fig. 6. Boiling curve experimental validation case [46] and the obtained results for a horizontal microchannel at a mass flux of 44.8 kg/m^{2}s and a range of heat fluxes which includes single-phase and two-phase experiments with FC-72.

effective heat flux was at its highest at the inlet and decreased along the channel length. Steeper downward gradients were present close to the vapour slug leading edge and where dry-out occurred. These trends were ascribed to the fluid or vapour's heat absorption ability at increased temperatures.

The average local bulk vapour quality plot illustrated in Fig. 7e follows directly from the energy balance analysis and exhibits an increasing trend. Notably, and as expected, neither the bubble nucleation sites nor the transient detached bubble locataions can be obtained from the local bulk vapour quality, however, the leading edge of the vapour slug was found to conicide well with calculated axial location where the vapour qaulity is zero.

As seen in Fig. 7f the local heat transfer coefficient increased within the single-phase region with sharp reductions being realised where the detached bubble and vapour slug resided. These trends align with what was found by previous researchers [1,6,7,42]. The further reduction in the heat transfer coefficients realised at the end of the channel where dry-out occurred could be expected due to vapour having significantly lower heat absorption capabilities.

From the above illustrations, it should be evident that the vapour and liquid distribution has a significant influence on the heat transfer performance. This can be ascribed to increased surface temperatures being realised at locations where vapour bubbles were present. It should be noted that the observed flow patterns varied for the different mass flux, heat flux and working fluid combinations. This highlights the importance of investigating the bubble dynamics to gain a better understanding of the associated local results.

6.3. Flow pattern observations

Intuitively, the flow pattern development and vapour slug length had a significant influence on the heat transfer coefficients obtained for the given geometry and mass and heat flux combinations. Typically, the heat transfer coefficients degraded substantially where the vapour slug resided, which resulted in reduced average heat transfer coefficients. Fig. 8 illustrates the typical flow patterns observed for all six working fluids at a mass flux of 15 kg/m^{2}s and similar average effective heat fluxes between 17.77 kW/m^2 and 18.42 kW/m^2. The observed flow patterns and boiling intensity differed for the respective working fluids considered at similar average heat fluxes due to the fluids exhibiting different saturation temperatures. In general, the flow patterns consisted of a liquid phase region and an elongated bubble (vapour slug), which was found in the outlet region. As seen in Fig. 8, the location and number of nucleation sites as well as the vapour slug lengths varied between the different fluid cases.

For the pure water case, the relatively low heat input resulted in only a few active nucleation sites. The bubble continued to grow progressively until it expanded into a vapour slug that occupied the outlet region. Due to pure ethanol exhibiting a lower saturation temperature and specific heat compared to that of the other fluids, pure ethanol achieved saturation conditions earlier (i.e. closer to the inlet) which caused more energy to be allocated to the phase-change process, resulting in a bigger vapour portion. For pure ethanol at $t = t_0 + 70$ ms, rapid bubble growth in the direction parallel to the flow created local liquid turbulence, which influenced the stability of the elongated bubble tail interface. As the bubble continued to grow, the coalescence of two elongated bubbles caused the occurrence of a mixing zone between the two bubbles, as shown in $t = t_0 + 76$ ms. This was followed by bubble expansion to the inlet region, which resulted in flow reversal and pressure fluctuations.

For the pure 1-butanol case, more active nucleation sites were present whilst a vapour slug resided in the outlet region. The nucleated bubbles grew due to the continuous heat input until bubble coalescence occurred. The same phenomenon was seen for the 5 % v/v ethanol-water binary mixture, however, the bubble which nucleated within the middle region of the channel grew and evolved into an elongated bubble before coalescence occurred at $t = t_0 + 124$ ms. This coalescence created a liquid-vapour mixing zone, which is often observed during churn flow. From inspection, it should be evident that neither of the 1-butanol-water self-rewetting fluid cases was dominated by nucleation events. Additionally, a unique feature of liquid entrainment within the vapour slugs was often observed for both of the 1-butanol-water self-rewetting fluid cases. This was caused by the merging of the liquid film above and below the bubble. During these flow boiling cases, the liquid-vapour interface experienced instability which formed a wavy interface at the bubble tail. Although the liquid film thickness could not be measured with the current experimental setup, the liquid entrainment could be an indication that an increased liquid film was found for the 1-butanol-water self-rewetting fluid cases than for any of the other working fluid cases. The presence of this liquid film was influential in postponing the direct contact between the vapour phase and the heated wall, effectively reducing the occurrence of dry-out and heat transfer performance deterioration.

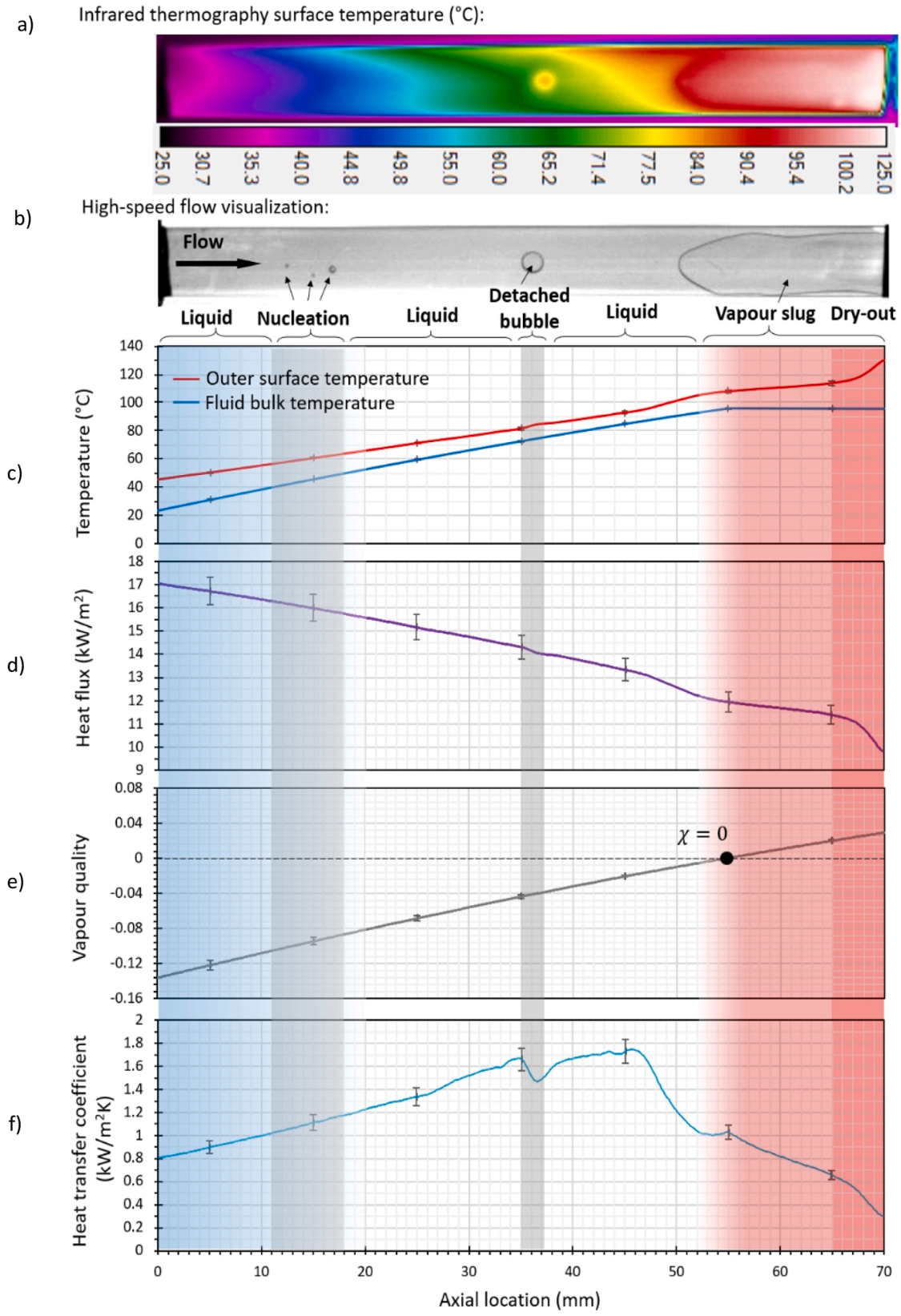

Fig. 7. The selected example test case results showcasing a) IR and b) HS camera footage and local width-wise average values of c) external surface and fluid temperatures, d) effective heat flux, e) vapour quality and f) overall heat transfer coefficient (based on external surface) for 5 % v/v 1-butanol-water at 10 kg/m^{2}s and 14.76 kW/m^2.

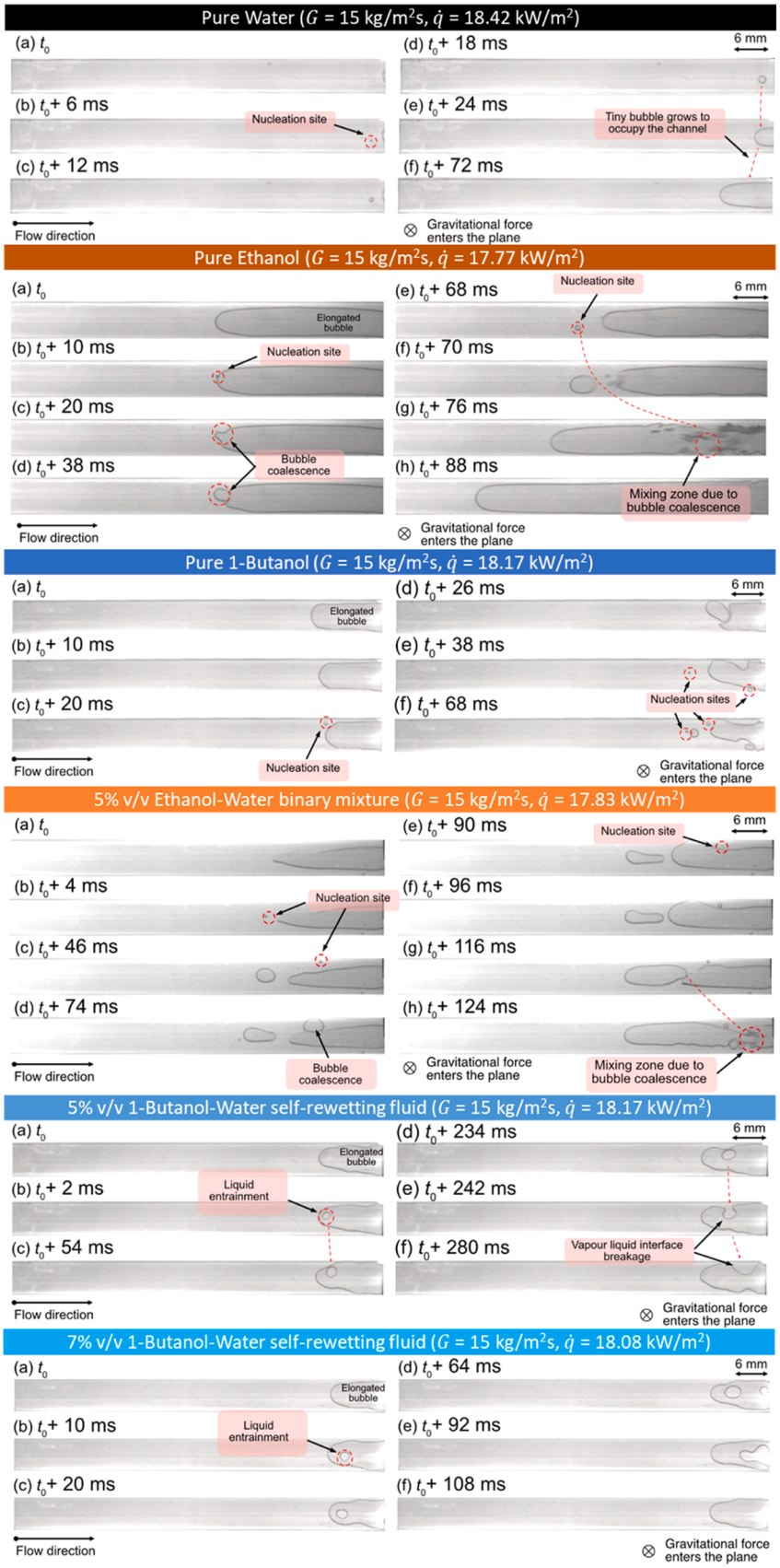

Fig. 8. Flow patterns observed during flow boiling of the respective fluids for a mass flux of 15 kg/m^{2}s at similar average effective heat fluxes between 17.77 kW/m^2 and 18.42 kW/m^2.

Fig. 9 provides an overview of the typical flow patterns observed during flow boiling experiments at higher average effective heat fluxes, specifically focussing on the effect that the addition of ethanol and 1-butanol to water had on the observed flow patterns. The illustrated cases, including pure water as a base case, were performed at a mass flux of 15 kg/m^{2}s and average effective heat fluxes between 23.77 kW/m^2 and 24.51 kW/m^2.

For all cases, increased vapour slug lengths were realised at higher average effective heat fluxes as increased heat caused more liquid to be converted into vapour which resulted in a larger vapour area being formed. For the pure water case, two bubbles nucleated within the middle region of the channel at $t = t_0 + 6$ ms. Bubble coalescence occurred at $t = t_0 + 20$ ms, where-after growth and expansion resulted in an elongated bubble forming. This expansion pushed the liquid between the bubble where-after further coalescence occurred, forming a single large vapour slug. This phenomenon was followed by flow reversal as seen between $t = t_0 + 98$ ms and $t = t_0 + 128$ ms. The mixing zone observed at $t = t_0 + 98$ ms could break the liquid film and trigger dry-out as suggested by a previous researcher [63].

For the ethanol-water binary mixture case, the vapour phase occupied almost the entire channel section, with the vapour slug being considerably larger than both other fluid cases performed at a similar average effective heat flux. Various nucleation sites were activated, affecting the vapour slug in various ways. As visible at $t = t_0$, the nucleation events took place close to the liquid-vapour interface of the elongated bubble. The bubble suddenly attached to the interface and merged without any significant influence on the interface stability. At $t = t_0 + 420$ ms, another nucleation site was found within the outlet region. In this case, the bubble merge created a small instability, which influenced the vapour-liquid interface, as observed at $t = t_0 + 442$ ms. Furthermore, a small bubble tail movement towards the channel inlet (i.e., opposite the flow direction) was also observed. The nucleation event observed at $t = t_0 + 508$ ms triggered other phenomena. Due to the rapid expansion of the small bubble, there was some disturbance in the liquid-vapour interface of the elongated bubble. A wavy interface was observed along the bubble, and a liquid-vapour mixing zone was observed within the outlet region. In addition, severe flow reversal took place in this region. As a result, a full vapour-dominant phase occupied the entire channel section, as observed at $t = t_0 + 526$ ms. The dominance of the vapour slug found in this case increased the probability of dry-out conditions.

For the 5 % butanol-water solution, a phenomenon similar to that at the lower average effective heat flux case was found. At $t = t_0 + 16$ ms the formation of liquid bridging in the middle of the elongated bubble was observed. The liquid region in the middle of the elongated bubble grew as it received more liquid from both the film below and above the bubble, where after, at $t = t_0 + 594$ ms the liquid finally broke the elongated bubble interface. The presence of liquid film between the bubble and the heated wall was considered important as it could prevent the occurrence of dry-out. Interestingly, the 5 % solution showed more

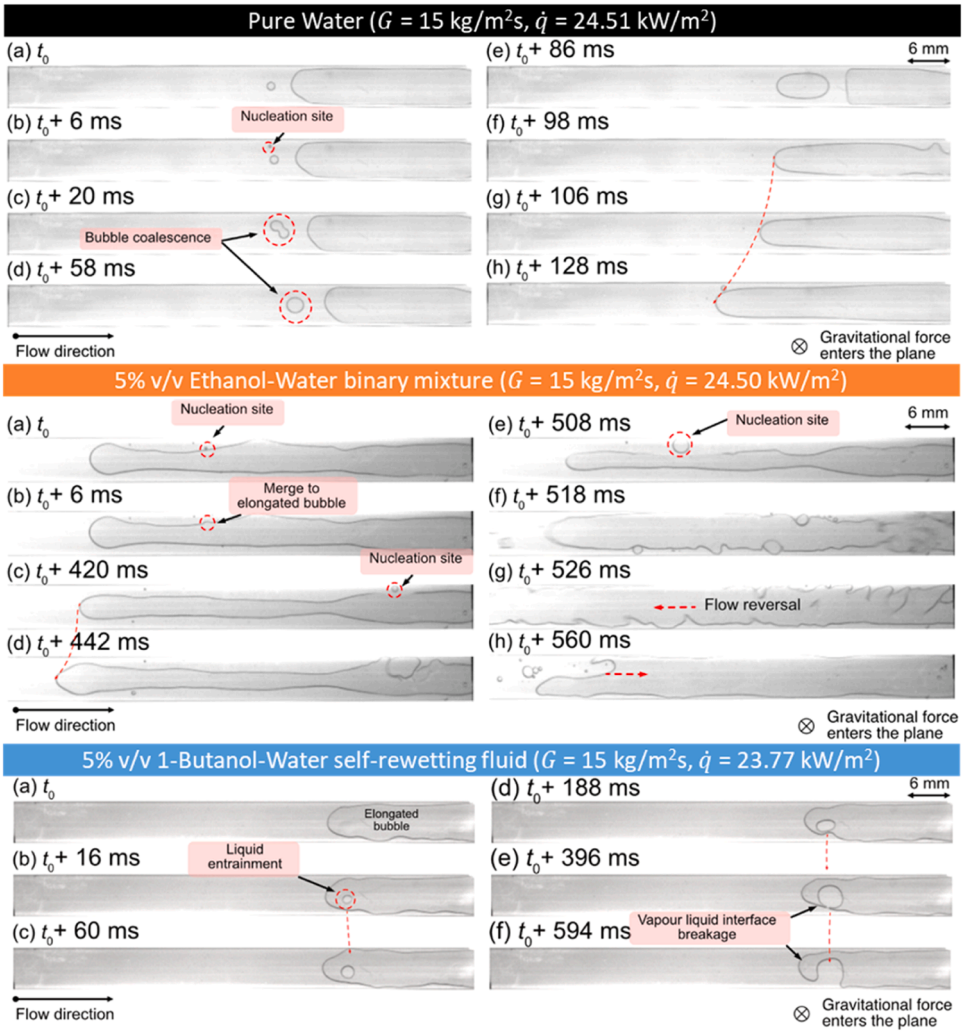

Fig. 9. Flow patterns observed during flow boiling of pure water, the 5 % v/v ethanol-water binary mixture and 5 % v/v 1-butanol-water self-rewetting fluid for a mass flux of 15 kg/m^{2}s at similar average effective heat fluxes between 23.77 kW/m^2 and 24.51 kW/m^2.

stable elongated bubble behaviour compared to the pure water and ethanol-water mixture at high average effective heat fluxes. As a result, flow reversal was minimal.

The data was also analysed for the slug regions only (and excluding the liquid-only regions) to determine the relative thermal performance of the fluids where the actual flow boiling occurred. Based on the flow visualizations, spatial averaging was done of the wall temperature and local heat transfer coefficients at the axial locations that were spanned by the vapour slugs. As illustrated previously, the vapour slug lengths differed for the respective working fluids and heat and mass flux combinations considered.

6.4. Wall temperature response

In general, across all fluids, an increase in the mass flux resulted in the decrease in the local wall temperatures and a delayed flow boiling initialisation along the flow channel length. In addition, and as expected, across all local vapour qualities an increase in the heat flux caused an increase in the local surface temperature. Fig. 10 presents the spatially averaged quasi steady state inner wall surface temperatures in the two-phase region ($\chi \geq 0$) against the spatially averaged two-phase region heat flux for all test fluids. For reference some data from the base fluids are also included. To reduce clutter, indicative uncertainty ranges are given at three different plotting locations. The sequence, from low to high, of the recorded wall temperatures corresponded broadly with the saturation temperatures of the different fluids. Pure ethanol, having the lowest saturation temperature produced the lowest wall temperatures, while on average the highest wall temperatures were obtained with pure 1-butanol. The butanol-water and ethanol-water mixtures operated in the same wall temperature band of between approximately 96 °C and 107 °C. At 10 and 15 kg/m^{2}s ethanol had the lowest wall temperatures, followed by the 5 % butanol-water mixture, while the 7 % butanol-water mixture produced the highest wall temperatures, irrespective of the heat flux. However, at the highest mass flux of 25 kg/m^{2}s the butanol mixtures had average wall temperatures that were approximately 6 °C cooler than the ethanol-water mixture. Additionally, no significant observable difference in the wall temperatures was noticed between the 5 % and 7 % concentrations at this mass flux. The average inner wall temperatures for the water cases were relatively scattered and ranged between 102 °C and 127 °C. Because of the relatively high saturation temperature of pure 1-butanol, limited data could be collected within the upper temperature restriction of the IR camera. The pure ethanol inner wall temperatures also exhibit a significant scatter and ranged between approximately 77 °C and 83 °C.

Even though variations in the wall temperature was observed as the heat flux was increased from one test case to the next, no observable correlation could be drawn between the wall temperatures for the pure substances (water, butanol and ethanol) and heat flux, particularly because of the scatter that was present in the data. However, for the butanol-water and ethanol-water mixtures, a direct influence on the wall temperature by the heat flux is present. An approximate linear dependency was observed within the test range as is indicated for the ethanol-water cases (as an example) by the purple line inserts in Fig. 10. The gradient of the linear fits for all of the mixtures are presented in Table 4. Based on the data, the ethanol-water mixture had on average the strongest wall temperature dependence on the heat flux.

Fig. 11 provides a broad overview of the inner wall temperatures for the butanol-water mixtures (both 5 % and 7 %), as well as for the ethanol-water mixture as obtained from the different mass flux test sets. For reference the average heat flux levels for each test set is also plotted and the standard variation magnitude of the wall temperatures are shown. As mentioned previously, both of the butanol-water mixtures showed a significant drop in the wall temperatures at the highest mass flux set compared to the lower mass fluxes, even though this set had the highest heat fluxes. Since there is a relatively weak coupling between the wall temperature and the heat flux, as is evident from the gradients in

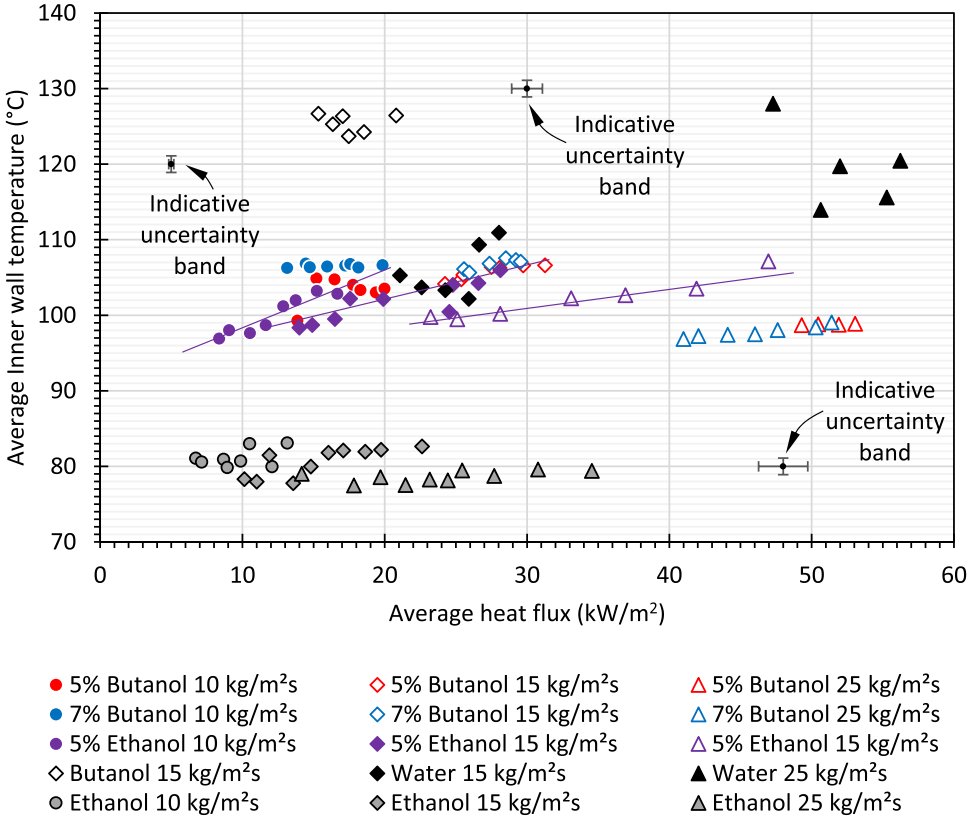

Fig. 10. Average surface temperatures in the two-phase flow boiling regions against the two-phase average heat flux for different fluids and mass fluxes.

Table 4
Approximate linear dependency of the spatially averaged inner wall temperature on the spatially averaged heat flux in the flow boiling regions of the butanol-water and ethanol-water mixtures.

	G, kg/m^{2}s	$\dot{q}_{ave}$, kW/m^2	Wall temperature gradient, °C/kW
5 % Butanol	10	16.5	0.34
	15	27.4	0.35
	25	50.3	0.22
7 % Butanol	10	16.4	0.03
	15	27.7	0.38
	25	50.3	0.18
5 % Ethanol	10	12.3	0.82
	15	20.8	0.43
	25	33.6	0.29

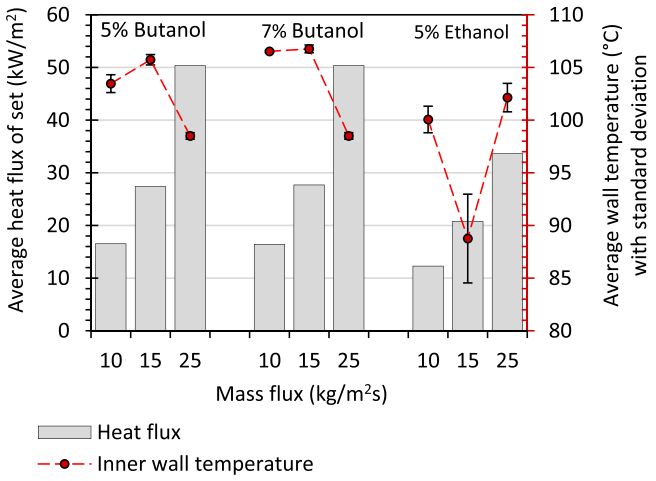

Fig. 11. Broad overview of average heat flux and average inner wall temperatures in the two-phase region in terms of mass flux for the butanol-water and ethanol-water mixtures.

Table 4, and since convective flow boiling is expected to improve with mass flux, the decrease in the wall temperature is probably due to the connective flow boiling phenomenon [1,2,6,7,42,64-66]. However, when comparing the 10 and 15 kg/m^{2}s cases for both of butanol-water mixtures, the increase in wall temperature from 10 to 15 kg/m^{2}s cannot be explained by improvements in convective flow boiling. If the relevant improvement is due to a nucleate boiling phenomenon, this could be associated with the self-rewetting nature and surface tension behaviour, which is expected to be most prevalent in low mass fluxes. Similar behaviour could not be observed when considering the ethanol-water mixture. Instead, the opposite occurred from 10 to 15 kg/m^{2}s.

6.5. Heat transfer performance

To establish whether there were observable trends in the heat transfer performance of the different fluids (pure substances and mixtures), the bulk saturation states were considered (vapour quality greater than zero), Eqs. (14) and (15) were applied respectively to determine the spatially averaged overall heat transfer coefficient (which includes the temperature difference of the glass wall), and the inner surface heat transfer coefficient.

The spatially averaged overall heat transfer coefficients in the saturation flow boiling regions of the test sections, and based on the outer measured wall temperature are presented in Fig. 12. Firstly, the overall heat transfer coefficients are considered to give an overview of the performance of the different fluids. To reduce clutter, indicative uncertainty range are included on the blue 7 % butanol-water data points only, but similarly sized uncertainties were achieved on the other data sets. Significant scatter in the obtained heat transfer coefficients, was observed particularly for the pure fluids (specifically water and ethanol). For this reason, data points are not graphically connected. However, where more definite trends are observable, data points are graphically connected as is evident in the results obtained for the 5 % and 7 % butanol-water mixtures (red and blue respectively), and to some extent for the ethanol-water mixture (purple).

When considering the 5 % and 7 % butanol-water mixtures at 10 kg/m^{2}s, an increased heat transfer performance is observed with an increase in heat flux. The approximated linear gradients for these two data sets are approximately 0.05 and 0.04 W/m^{2}K per W/m^2 respectively indicating a mild improvement with heat flux, which is not mass flux dependent. At 15 and 25 kg/m^{2}s such a dependence outside the uncertainty bands could not be observed.

Surface tension effects have previously been reported to play a significant role in the heat transfer performance during microchannel flow boiling investigations [67]. As was shown in Fig. 1, the surface tension profiles for the 5 % and 7 % butanol-water solutions have an upward trend at temperatures of 60 °C and above. Self-rewetting due to the Marangoni effect could be prevalent and significant enough to explain this heat transfer performance improvement where progressively hotter fluids (as would be the case with increased heat flux) experiences higher surface tension and probable better rewetting and reduced tendencies for local dry-out between the vapour slug and the hot surface. The other fluids do not have this surface-tension temperature dependency.

Besides for butanol-water at 25 kg/m^{2}s, the mixtures had lower heat transfer coefficients compared to their pure substance counterparts. Based on the data, pure ethanol had the highest heat transfer coefficient, and the butanol-water mixtures had the lowest heat transfer coefficient (except at 25 kg/m^{2}s). Even though the butanol-water mixtures exhibited lower heat transfer coefficients than for instance water, the repeatable and predictable behaviour is a great advantage and indicates that the influence of or prevalence of flow instabilities have been significantly mitigated as was observed from the flow visualisations.

A region of interest that focuses on the data range of the butanol-water and ethanol-water mixtures are presented in Fig. 13 where the spatially average inner surface heat transfer coefficient in the saturation flow boiling portions of the test sections are presented. As previously, indicative uncertainty bands are shown on the 7 % butanol-water data only to reduce clutter. The plotted data was obtained from Eq. (15) after the temperature difference over the glass wall was taken into consideration. Because the overall heat transfer coefficient (presented previously) includes the relatively weak thermal conductivity mechanism in the wall, the inner surface heat transfer coefficients are naturally greater. Its relative magnitude depends on the dominance of the conduction and convective thermal resistances that operated in series. The heat transfer performance dependence on the heat flux is particularly noticeable for the butanol-water mixtures. After removing the wall conduction effects, the approximated linear gradients of the inner wall heat transfer coefficients to heat flux doubles to approximately 0.1 and 0.07 W/m^{2}K per W/m^2 respectively.

A summary of the averaged heat transfer coefficient for each data set of the butanol-water and ethanol-water mixtures are presented in Fig. 14a for easier comparison. The averaged overall and inner surface heat transfer coefficients and heat fluxes from Fig. 12 and Fig. 13 are plotted for each mass flux case. The standard deviations on in the data from which each average is drawn, are also shown. For all three fluid mixtures the heat transfer coefficients increased with mass flux. At 25 kg/m^{2}s the 5 % butanol-water mixture had the highest average inner heat transfer coefficient, which was approximately 140 % higher than for the ethanol-water mixture and 22 % higher than for the 7 % butanol-water mixture.

A direct comparison between the inner surface heat transfer coefficients of two butanol-water mixtures is presented in Fig. 14b. For all three mass fluxes, the 5 % butanol-water mixtures outperformed the 7 % butanol-water mixture. Compared to the 7 % concentration case, 5 % butanol water exhibited heat transfer coefficient improvements of

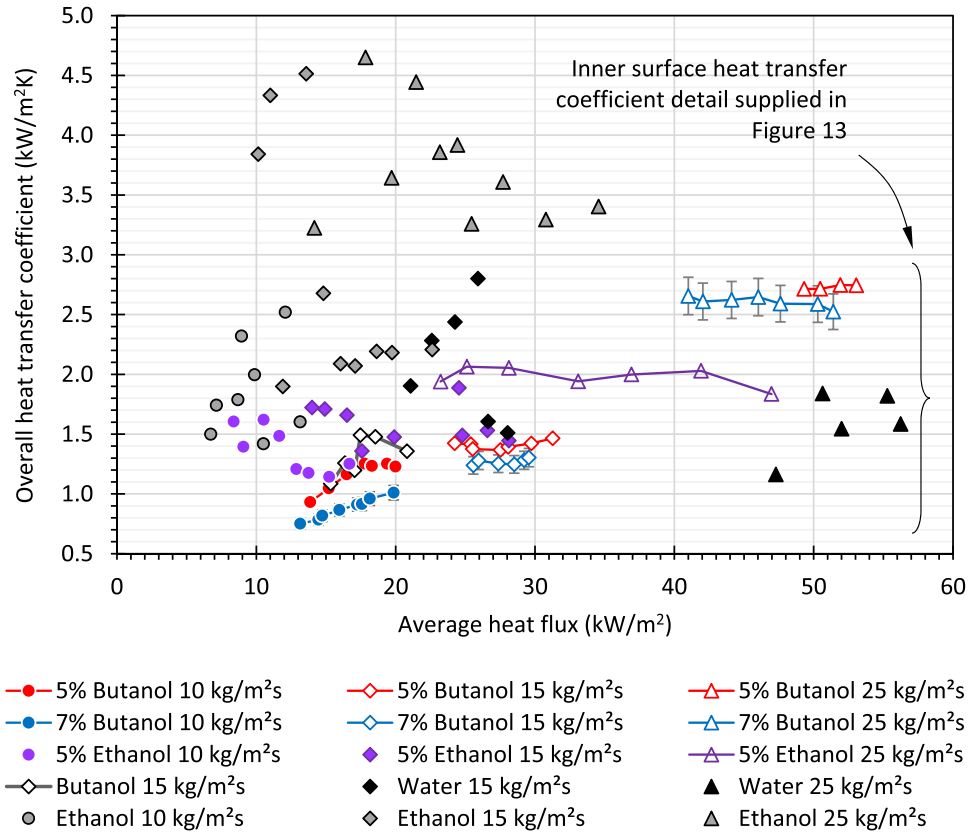

Fig. 12. Spatially averaged overall heat transfer coefficients in the saturated flow boiling region based on the exterior wall temperature in terms of the average heat flux for each fluid and mass flux test case set.

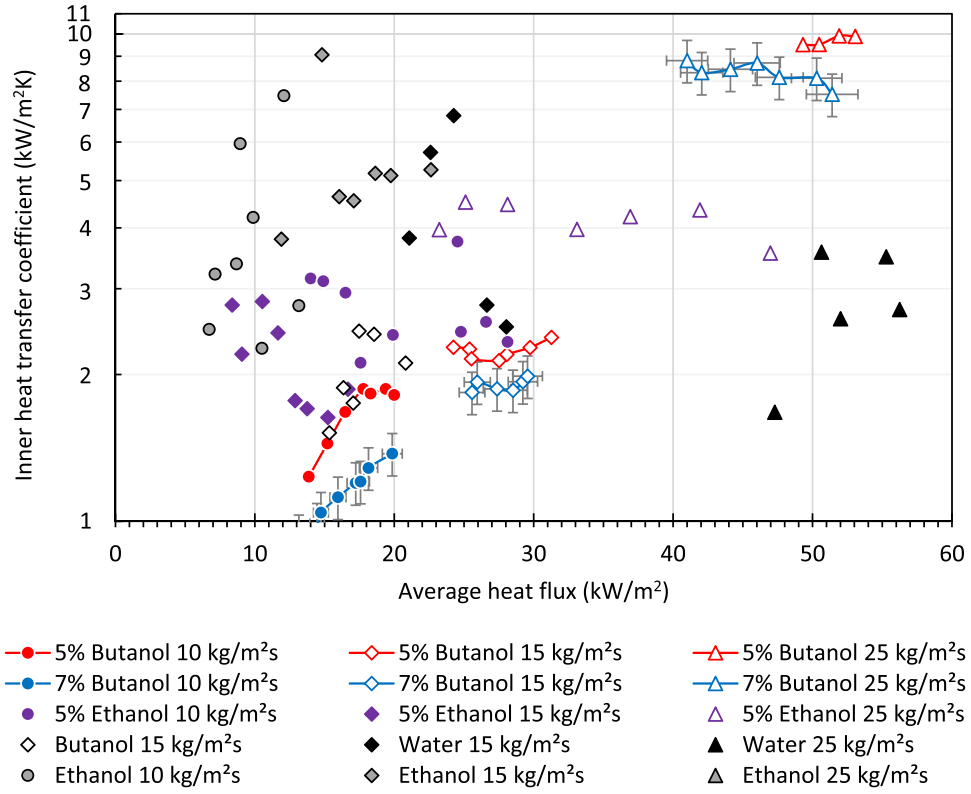

Fig. 13. Spatially averaged inner surface heat transfer coefficients in the saturated flow boiling region in terms of the average heat flux for each fluid and mass flux test case set.

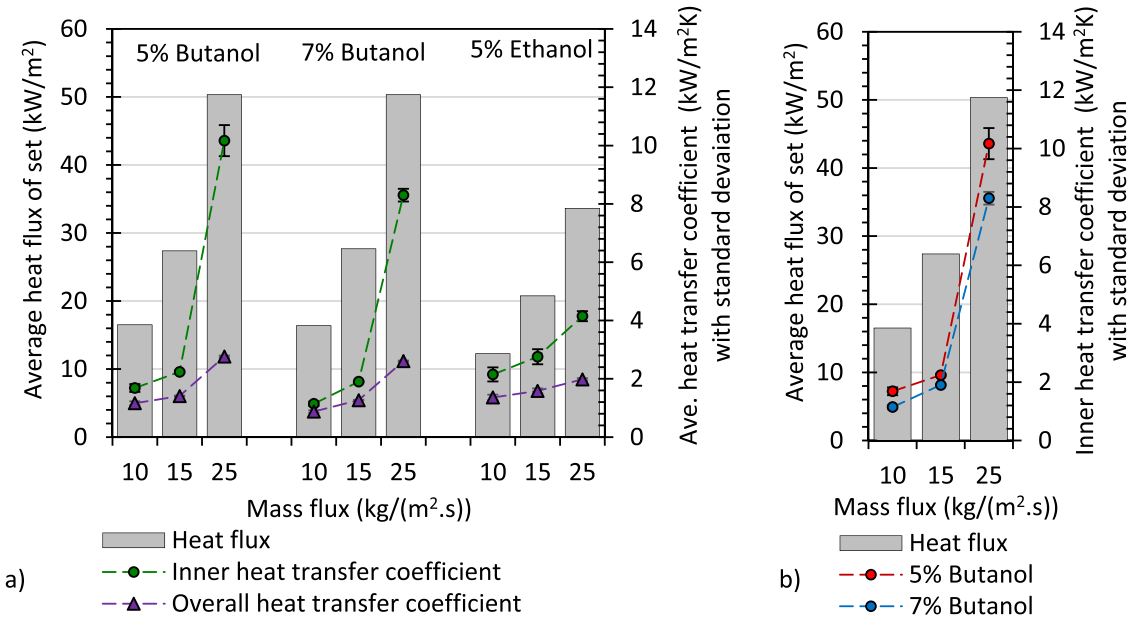

Fig. 14. Broad overview of average heat flux and average heat transfer coefficient (overall and based on the inner surface) in the two-phase region in terms of mass flux for a) the butanol-water and ethanol-water mixtures, and b) direct comparison between inner heat transfer coefficients of the 5 % and 7 % butanol-water mixture cases.

between 17 % and 47 %. Based on this, it can be deduced that an optimal solution composition should exist, which falls beyond the scope of this study. This aligns with a previous study that found that transition concentrations exist, depending on the balance of thermal and solutal-Marangoni forces [21].

7. Conclusions

This experimental study considered six working fluids including pure water, pure 1-butanol, pure ethanol, dilute butanol-water self-rewetting (5 % and 7 % by volume butanol) and dilute ethanol-water binary (5 % by volume ethanol) mixtures. Locally uniform one-sided electric heating was applied to a borosilicate glass microchannel with a width and height of 6 mm and 0.3 mm, respectively, yielding a high aspect ratio of 20. Three relatively low mass fluxes of 10, 15 and 25 kg/m^{2}s over a range of applicable heat fluxes at a horizontal orientation were considered for each fluid mixture. Local and average wall temperatures and heat transfer were obtained and considered against the governing flow pattern visualisations.

It was found that fluid type and by hypothesis, the surface tension effects via the Marangoni principle, have a significant influence on the heat transfer coefficients realised during microchannel flow boiling. Specifically, self-rewetting fluids with non-linear surface tension profiles, proved to exhibit the potential of yielding high heat transfer coefficients at increased heat fluxes. The following summary of conclusions could be raked from the working fluid investigation performed:

- In terms of the wall temperature response, the ethanol-water binary and 1-butanol-water self-rewetting mixtures operated in the same temperature band of 96 °C and 107 °C, with the 7 % butanol-water self-rewetting mixture producing the highest wall temperatures, irrespective of the heat flux.
- The spatially averaged overall heat transfer coefficients in the saturated flow boiling region based on the exterior wall temperature illustrated that the 1-butanol-water self-rewetting mixture obtained increased heat transfer performance at a mass flux of 10 kg/m^{2}s with an increase in heat flux, whist the same dependence was not evident at the higher mass fluxes.
- Based on the overall heat transfer coefficients, pure ethanol had the highest heat transfer coefficient and the 1-butanol-water mixtures exhibited the lowest heat transfer coefficient (except at 25 kg/m^{2}s), however, flow instability was significantly mitigated by the 1-butanol-water self-rewetting mixtures.
- The 5 % 1-butanol-water self-rewetting mixture obtained the highest average inner surface heat transfer coefficient which was approximately 140 % higher than that of the ethanol-water binary mixture at a mass flux of 25 kg/m^{2}s.
- Between the different 1-butanol-water self-rewetting concentrations, the 5 % concentration case produced 17 % to 47 % higher average inner surface heat transfer coefficients than the 7 % concentration case.
- Based on the flow visualisations, 1-butanol-water self-rewetting mixtures produced an adequate liquid film between the bubble and heated wall, resulting in entrained liquid within vapour slugs and reducing dry-out.

This experimental investigation illustrated the thermal management potential when implementing 1-butanol-water self-rewetting mixtures as a working fluid for microchannel flow boiling applications. The 5 % v/v 1-butanol-water self-rewetting mixture not only demonstrated that increased two-phase heat transfer coefficients could be obtained at significantly higher effective heat fluxes for low mass flux conditions, but also that the crucial problem of dry-out could be reduced significantly by utilising self-rewetting fluids as opposed to pure substances.

CRediT authorship contribution statement

Mandi Venter: Writing – original draft, Investigation, Formal analysis. **Arif Widyatama:** Writing – original draft, Visualization, Investigation. **Jaco Dirker:** Writing – review & editing, Supervision, Conceptualization. **Khellil Sefiane:** Writing – review & editing, Supervision, Resources, Conceptualization.

Declaration of competing interest

The authors declare that they have no known competing financial interests or current personal relationships that could have appeared to

influence the work reported in this paper.

Data availability

Data will be made available on request.

Acknowledgements

The authors acknowledge the EC-RISE-ThermaSMART project that was funded by the European Union's Horizon 2020 research and innovation programme under the Marie Skłodowska-Curie grant agreement No. 778104.

References

[1] T.G. Karayiannis, M.M. Mahmoud, Flow boiling in microchannels: fundamentals and applications, Appl. Therm. Eng. 115 (2017) 1372–1397.
[2] S.K. Saha, Microchannel Phase Change Transport Phenomena, Oxford, UK, 2015, pp. 1–2.
[3] Hong, S., Zhang, B., Dang, C., and Hihara, E., Development of two-phase flow microchannel heat sink applied to solar-tracking high-concentration photovoltaic thermal hybrid system. 2020. Volume 212(118739).
[4] P.A. Kew, K. Cornwell, Correlations for the prediction of boiling heat transfer in small-diameter channels, Appl. Therm. Eng. 17 (8–10) (1997) 705–715.
[5] N. Brauner, D.M. Maron, Identification of the range of small diameter conduits regarding two-phase flow pattern transitions, Int. Commun. Heat Mass Transf. 19 (1) (1992) 29–39.
[6] L. Cheng, G. Xia, Fundamental issues, mechanisms and models of flow boiling heat transfer in microscale channels, Int. J. Heat. Mass Transf. 108 (2017) 97–127.
[7] M.R. Özdemir, M.M. Mahmoud, T.G. Karayiannis, Flow boiling of water in a rectangular metallic microchannel, Heat Transf. Eng. 42 (6) (2021) 492–516.
[8] H.J. Kim, L. Liebenberg, A.M. Jacobi, Flow visualization of two-phase R-245fa at low mass flux in a plate heat exchanger near the micro-macroscale transition, Sci. Technol. Built. Environ. 25 (10) (2019) 1292–1301.
[9] Wei Li, A general criterion for evaporative heat transfer in micro/mini-channels, Int. J. Heat. Mass Transf. 53 (2010) 1967–1976. Issues 9–10.
[10] H.J. Kim, L. Liebenberg, A.M. Jacobi, Convective boiling of R-134a near the micro-macroscale transition inside a vertical brazed plate heat exchanger, J. Heat Mass Transf. 140 (9) (2018) 6–10.
[11] S.S. Mehendale, A.M. Jacobi, R.K. Shah, Fluid flow and heat transfer at micro- and meso-scales with application to heat exchanger design, Appl. Mech. Rev. 53 (7) (2000) 175–193.
[12] ASHRAE, Natural Refrigerants, 2011. Available from, https://www.epa.gov/sites/default/files/documents/ASHRAE_PD_Natural_Refrigerants_2011.pdf.
[13] D. Mikielewicz, J. Wajs, M. Gliński, A.-B.R.S. Zrooga, Experimental investigation of dryout of SES 36, R134a, R123 and ethanol in vertical small diameter tubes, Exp. Therm. Fluid Sci. 44 (2013) 556–564.
[14] S. Cao, H. Yang, L. Zhao, T. Wang, J. Xie, Recent advances of surface wettability effect on flow boiling heat transfer performance, Front. Heat Mass Transf. 17 (17) (2021).
[15] S.G. Kandlikar, W.K. Kuan, D.A. Willistein, J. Borrelli, Stabilization of flow boiling in microchannels using pressure drop elements and fabricated nucleation sites, ASME J. Heat Mass Transf. 128 (4) (2006) 389–396.
[16] S.S. Bertsch, E.A. Groll, S.V. Garimella, Refrigerant flow boiling heat transfer in parallel microchannels as a function of local vapor quality, Int. J. Heat. Mass Transf. 51 (19–20) (2008) 4775–4787.
[17] J. Xu, Y. Wang, R. Yang, W. Liu, H. Wu, Y. Ding, Y. Li, A review of boiling heat transfer characteristics in binary mixtures, Int. J. Heat. Mass Transf. 164 (2021).
[18] D. Mamalis, V. Koutsos, K. Sefiane, Bubble rise in a non-isothermal self-rewetting fluid and the role of thermocapillarity, Int. J. Therm. Sci. 117 (2017) 146–162.
[19] Y. Abe, A. Iwaski, K. Tanaka, Thermal management with self-rewetting fluids, Micrograv. Sci. Technol. 16 (2005) 148–152.
[20] A. Sitar, I. Golobic, Heat transfer enhancement of self-rewetting aqueous n-butanol solutions boiling in microchannels, Int. J. Heat. Mass Transf. 81 (2015) 198–206.
[21] K. Namura, K. Nakajima, M. Suzuki, Investigation of transition from thermal- to solutal-Marangoni flow in dilute alcohol/water mixtures using nano-plasmonic heaters, Nanotechnology. 29 (6) (2018).
[22] M. Shanahan, K. Sefiane, Recalcitrant Bubbles, 4, Scientific Reports, 2014, p. 4727.
[23] G. Vázquez, E. Alvarez, J.M. Navaza, Surface Tension of alcohol + Water from 20 to 50°C, J. Chem. Eng. Data 40 (3) (1995) 611–614.
[24] Springer Materials. Surface tension of water, ethanol, 1-butanol, water-ethanol mixture, water-butanol mixtures. 2023; Available from: https://materials.springer.com/interactive?systemId=16910&propertyId=Surface%20Tension, https://materials.springer.com/interactive?systemId=16598&propertyId=Surface%20Tension, https://materials.springer.com/interactive?systemId=1838&propertyId=Surface%20Tension, https://materials.springer.com/interactive?systemId=215&propertyId=Surface%20Tension, https://materials.springer.com/interactive?systemId=3860&propertyId=Surface%20Tension.
[25] L. Cheng, D. Mewes, Review of two-phase flow and flow boiling of mixtures in small and mini channels, Int. J. Multiphase Flow 32 (2) (2006) 183–207.
[26] M.C. Vlachou, T.D. Karapantsios, Effect of channel inclination on heat transfer and bubble dynamics during subcooled flow boiling, Int. J. Therm. Sci. 124 (2018) 484–495.
[27] K. Strąk, M. Piasecka, B. Maciejewska, Spatial orientation as a factor in flow boiling heat transfer of cooling liquids in enhanced surface minichannels, Int. J. Heat. Mass Transf. 117 (2018) 375–387.
[28] P. Vasileiadou, K. Sefiane, T.G. Karayiannis, J.R.E. Christy, Flow Boiling of Ethanol/Water Binary Mixture in a Square Mini-Channel, 127, Applied Thermal Engineering, 2017, pp. 1617–1626.
[29] M.S. Tsou, B.R. Fu, C. Pan, Critical heat flux on flow boiling of ethanol–water mixtures in a diverging microchannel with artificial cavities, in: 8th International Conference on Heat Transfer, Fluid Mechanics and Thermodynamics, 2011, p. 9.
[30] M. Kuramae, M. Suzuki, Two-component heat pipes utilizing the Marangoni effect, Chem. Eng. 26 (2) (1993) 230–231.
[31] N. Ono, A. Hamaoka, Y. Eda, K. Obara, High-carbon alcohol aqueous solutions and their application to flow boiling in various mini-tube systems. Evaporation, Condensation and Heat Transfer, IntechOpen, 2011, pp. 465–485.
[32] M. Talebi, S. Sadir, M. Kraut, R. Dittmeyers, P. Woias, Local heat transfer analysis in a single Microchannel with boiling DI-water and correlations with impedance local sensors, Energies (Basel) 13 (23) (2020) 6473.
[33] Y.Q. Xie, J.Z. Yu, Z.H. Zhao, Experimental investigation of flow and heat transfer for the ethanol-water solution and FC-72 in rectangular microchannels, Int. J. Heat. Mass Transf. 41 (2005) 695–702.
[34] X. Cheng, H. Wu, Improved flow boiling performance in high-aspect-ratio interconnected microchannels, Int. J. Heat. Mass Transf. 165 (2021) 120627. Paper.
[35] Q. Zhao, D. Zhang, J. Qiu, M. Lu, J. Zhou, X. Chen, Bubble behaviors and flow boiling characteristics in open microchannels with large aspect ratio, Appl. Therm. Eng. 213 (2022) 118768. Paper.
[36] J. Barber, K. Sefiane, D. Brutin, L. Tadrist, Hydrodynamics and heat transfer during flow boiling Instabilities in a single microchannel, Appl. Therm. Eng. 29 (7) (2009) 1299–1308.
[37] J. Barber, D. Brutin, K. Sefiane, L. Tadrist, Bubble confinement in flow boiling of FC-72 in a "rectangular" microchannel of high aspect ratio, Exp Therm Fluid Sci 34 (8) (2010) 1375–1388.
[38] K.S. Jacqueline Barber, David Brutin, Lounes Tadrist, Hydrodynamics and heat transfer during flow boiling instabilities in a single microchannel, Appl. Therm. Eng. 29 (7) (2009) 1299–1308.
[39] J. Barber, D. Brutin, K. Sefiane, J.L. Gardarein, L. Tadrist, Unsteady-state fluctuations analysis during bubble growth in a "rectangular" microchannel, Int. J. Heat. Mass Transf. 54 (23–24) (2011) 4784–4795.
[40] S. Korniliou, Local Heat Transfer Measurements and Aspect Ratio Influence During Flow Boiling in Microscale, The University of Edinburgh, 2018.
[41] S. Korniliou, Experimental Study on Local Heat Transfer Coefficients and the Effect of Aspect Ratio on Flow Boiling in a Microchannel, in Engineering, University of Edinburgh, 2017.
[42] M. Vermaak, J. Potgieter, J. Dirker, M.A. Moghimi, P. Valluri, K. Sefiane, J. P. Meyer, Experimental and numerical investigation of Micro/Mini channel flow-boiling heat transfer with non-uniform circumferential heat fluxes at different rotational orientations, Int. J. Heat. Mass Transf. 158 (2020).
[43] S. Korniliou, C. Mackenzie-Dover, S. Harmand, G. Duursma, J.R.E. Christy, J. G. Terry, A.J. Walton, K. Sefiane, Local wall temperature mapping during flow boiling in a transparent microchannel, Int. J. Therm. Sci. 135 (2019) 344–361.
[44] Y. Wang, Liquid-Vapour Phase Change and Multiphase Flow Heat Transfer in Single Micro-Channels Using Pure Liquids and Nano-Fluids, in Engineering, University of Edinburgh, 2011.
[45] Y. Wang, K. Sefiane, S. Harmand, Flow boiling in high-aspect ratio mini- and micro-channels with FC-72 and ethanol: experimental results and heat transfer correlation assessments, Exp. Therm. Fluid Sci. 36 (2012) 93–106.
[46] Y. Wang, K. Sefiane, Effects of heat flux, vapour quality, channel hydraulic diameter on flow boiling heat transfer in variable aspect ratio micro-channels using transparent heating, Int. J. Heat. Mass Transf. 55 (9–10) (2012) 2235–2243.
[47] R.P. Madding, Emissivity measurement and temperature correction accuracy considerations, in: SPIE Conference on Thermosense XXI 3700, 1999.
[48] Infrared Thermography. Emissivity values for common materials. Available from: https://www.thermoworks.com/emissivity-table/.
[49] V.Y.S. Lee, T.G. Karayiannis, Effect of inlet subcooling on flow boiling in microchannels, Appl. Therm. Eng. 181 (2020).
[50] R. Prattipati, S. Pendyala, B.V.S.S.S. Prasad, Void fraction in helical coils during flow boiling with inlet subcooling, Int. J. Heat. Mass Transf. 168 (2021).
[51] C.H. Hoang, S. Rangarajan, S. Khalili, B. Ramakrisnan, V. Radmard, Y. Hadad, S. Schiffres, B. Sammakia, Hybrid microchannel/multi-jet two-phase heat sink: a benchmark and geometry optimization study of commercial product, Int. J. Heat. Mass Transf. 169 (2021).
[52] S.J. McPhail, Single-phase Fluid Flow and Heat Transfer in Microtubes, Stuttgart University, 2008.
[53] Y. Li, H. Wu, Y. Yao, Enhanced flow boiling heat transfer and suppressed boiling instability in counter-flow stepped microchannels, Int. J. Heat. Mass Transf. 194 (2022).
[54] K. Luo, W. Li, J. Ma, W. Chang, G. Huang, C. Li, Silicon microchannels flow boiling enhanced via microporous decorated sidewalls, Int. J. Heat. Mass Transf. 191 (2022).
[55] W. Li, K. Luo, C. Li, Y. Joshi, A remarkable CHF of 345W/cm2 is achieved in a wicked-microchannel using HFE-7100, Int. J. Heat. Mass Transf. 187 (2022).

[56] G. Criscuolo, W.B. Markussen, K.E. Meyer, M.R. Kærn, High heat flux flow boiling of R1234yf, R1234ze(E) and R134a in high aspect ratio microchannels, Int. J. Heat. Mass Transf. 186 (2022).
[57] Thermtest Instruments, Rule of Mixtures Calculator, 2021. Available from, https://thermtest.com/thermal-resources/rule-of-mixtures.
[58] Tamu Education, Chapter 5: The Thermodynamic Description of Mixtures, 2005. Available from, https://www.chem.tamu.edu/class/majors/chem328/CHEM%20328_Chapter%2005.pdf.
[59] Martinez, I. Mixtures. Available from: http://imartinez.etsiae.upm.es/~isidoro/bk3/c07/Mixtures.pdf.
[60] Asada, M. Material Characterization of Alcohol-Water mixtures for the numerical simulation of heat transfer in micro-channels. 2012; Available from: https://www.semanticscholar.org/paper/Material-characterization-of-alcohol-water-mixtures-Asada/27b8d17f36328cf582f1e80c17e68c6d3afd4e77.
[61] R. Waller, T. Strang, Physical chemical properties of preservative solutions - ethanol-water solutions, Collection Forum 12 (2) (1996) 70–85.
[62] V. Lindberg, Uncertainties and Error Propagation Part I of a Manual on Uncertainties, Graphing, and the Vernier Caliper, 2000. Available from, https://www.geol.lsu.edu/jlorenzo/geophysics/uncertainties/Uncertaintiespart2.html.
[63] B.R. Fu, P.H. Lin, M.S. Tsou, C. Pan, Flow pattern maps and transition criteria for flow boiling of binary mixtures in a diverging microchannel, Int. J. Heat. Mass Transf. 55 (5–6) (2012) 1754–1763.
[64] S.M. Ghiaasiaan, Two-phase Flow Boiling and Condensation in Conventional and Miniature Systems, Cambridge University Press, 2008.
[65] A. Faghri, Y. Zhang, Transport Phenomena in Multiphase Systems, Int. J. Heat. Mass Transf. 50 (2006) 765–852.
[66] L.S. Tong, Y.S. Tang, Boiling Heat Transfer and Two-phase Flow, Taylor & Francis, 2017.
[67] Y.W. Na, Forced Convection Flow Boiling and Two-Phase Flow Phenomena in a Microchannel, University of Florida, 2008.